Material Characterization and Testing of Cured-in-Place Pipe to Resist Earthquake Related Ground Deformation

A Thesis

Presented to the Faculty of the Graduate School

of Cornell University

In Partial Fulfillment of the Requirements for the Degree of

Master of Science

by

Natalie Lucia Mottl

August 2019

ABSTRACT

This thesis summarizes the testing procedures and key results of full-scale tests on Cured-In-Place Pipe (CIPP) to evaluate its performance under earthquake induced ground deformation. The CIPP used in this work is commercially available as Aqua-pipe, manufactured by Sanexen Environmental Services, Inc. to rehabilitate water mains. The investigation covered in this work includes tensile coupon tests, direct tension tests, friction tests, and direct shear tests. The test results improve the understanding and characterization of the axial force vs. displacement relationship for CIPP movement relative to the host pipe, lining/pipe interface friction, and the effects of geometry, internal pressure, and repeated loading on the axial force vs. relative displacement relationship.

The direct tension test results show that the mobilization of axial force is affected by Mode II fracture propagation, friction between the exterior surface of the lining and interior surface of the host pipe, and geometric resistance generated by the relative movement of the lining within a host pipe of variable inside diameter. The most important finding from the direct tension tests is that substantial additional axial forces may be mobilized after debonding as the lining is affected by geometric interference caused by movement through a pipe with variable internal diameter. The test results provide a first-time confirmation of this loading mechanism.

The friction tests show that the axial load response is independent of loading rate, with a similar load range and maximum load for the tests conducted at 1 in. (25 mm)/min, 10 in. (250 mm)/min, and 100 in. (2500 mm)/min. The first friction test, done under no pressure, developed larger axial forces due to the greater frictional resistance between the lining and pipe than in a subsequent test under the same testing conditions and

geometry. The difference in the axial loads show that overcleaned field pipes or new ductile iron pipes can have a greater frictional resistance between the lining and pipe than properly cleaned or previously loaded pipes. The most important result from the friction tests involves the influence of internal pressure on axial load response. As the internal pressure increased, the axial load for a given displacement increased linearly. Regressions of axial load vs. internal pressure at the same levels of displacement show a clear linear relationship with similar slopes.

The results of the direct shear tests for new ductile iron and field cast iron pipes show a coefficient of friction of 0.61. This value represents the relatively smooth debonded lining surface conditions representative of the CIPP cleaning and lining process for old cast iron water mains. It also represents the interface between the lining and new ductile iron pipe after repeated displacements. The test results show that a coefficient of friction of 0.84 is a good estimate for lining/pipe interfaces that are rough and irregular.

BIOGRAPHICAL SKETCH

Natalie Mottl completed a Bachelor's Degree in Civil Engineering at Cornell University in May 2018. She is currently a degree candidate for a Master's Degree in Civil Engineering at Cornell Engineering with an expected graduation date in August 2019. During her time at Cornell University, she was a part of AguaClara, a water treatment research group and worked with Professor O'Rourke and Professor Stewart in the geotechnical engineering lab group.

ACKNOWLEDGMENTS

The author recognizes the excellent efforts of Cornell faculty and graduate, undergraduate, and other students who made these experiments successful. Professor T.D. O'Rourke was the M.S. thesis advisor, and Professor H.E. Stewart was the other member of the Thesis Committee. The contributions to the full-scale CIPP testing of Dakota Price, Jim Straight, Mia Stewart, Sarah Weinberg, Corbin Atkins, Quinton Hubbell, George Howell III, Andrew Greubel, Daniel Kusky, and Dara Karać are acknowledged.

TABLE OF CONTENTS

LIST OF FIGURES

LIST OF TABLES

CHAPTER 1

INTRODUCTION

This thesis presents the results of material property and full-scale testing to characterize the performance of Cured-in-Place Pipe (CIPP). The CIPP used in this work is available commercially as Aqua-pipe, developed by Sanexen Environmental Services, Inc. to rehabilitate water pipelines as an alternative to pipeline removal and replacement. Sanexen is an environmental services contractor based in Canada with a counterpart in the U.S., Sanexen Water.

As shown in Figure 1.1, Aqua-pipe is an epoxy resin-impregnated lining consisting of an inner and outer layer, or jacket, each composed of woven fabric. Each layer of woven fabric consists of polyethylene thermoplastic (PET) yarns in the longitudinal, or warp, direction and PET yarns in the circumferential, or weft, direction, as shown in the warp and weft schematic in Figure 1.2. There are 23 yarns/in. in the warp direction and 8.5 yarns/in. in the weft direction in the Aqua-pipe fabric. The yarns in the warp direction are a discontinuous filament, while the yarns in the weft direction are continuous and stronger than those in the warp direction. The ratio of stress at failure for the weft vs. warp direction is 1.39 according to data provided by the manufacturer. A layer of epoxy is located between the two jackets. The interior layer of the lining is composed of a polyurethane waterproof membrane. Figure 1.3 shows the two layers of woven fabric before being treated with epoxy and cured in place. Figure 1.4 shows Aqua-pipe after curing inside of an existing pipeline.

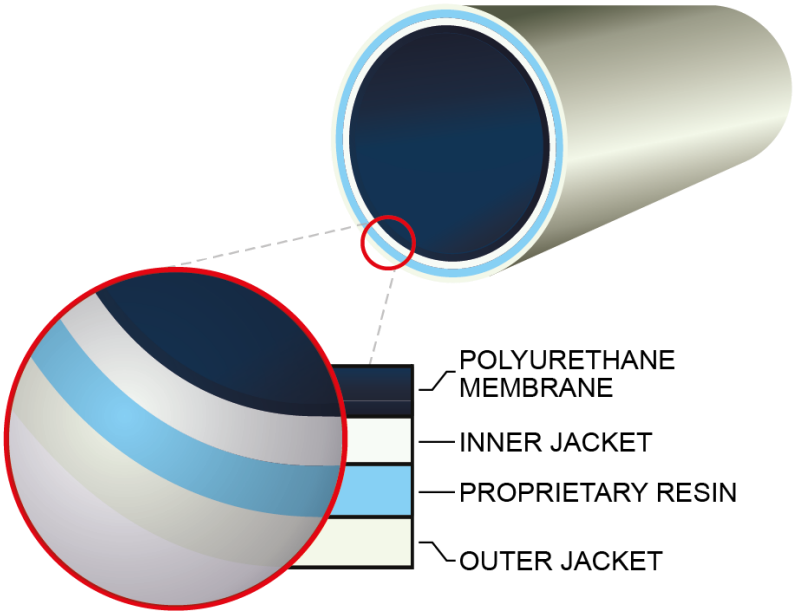

Figure 1.1. Aqua-pipe Geotextile Lining Components

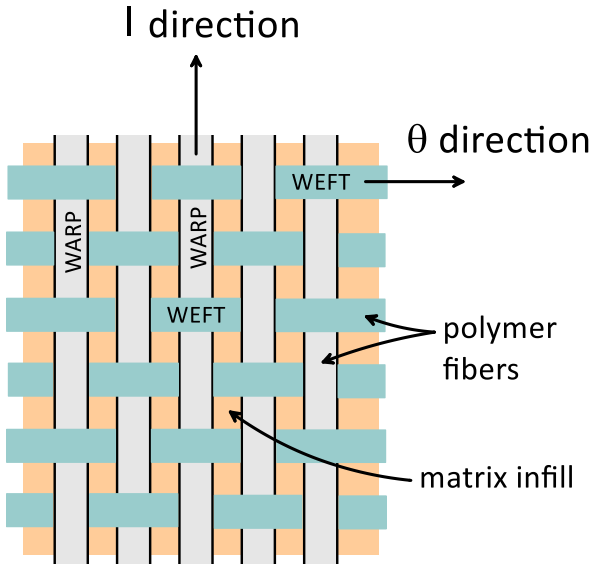

Figure 1.2. Schematic of Warp and Weft Yarn Pattern

Figure 1.3. Aqua-pipe Geotextile Lining before Curing

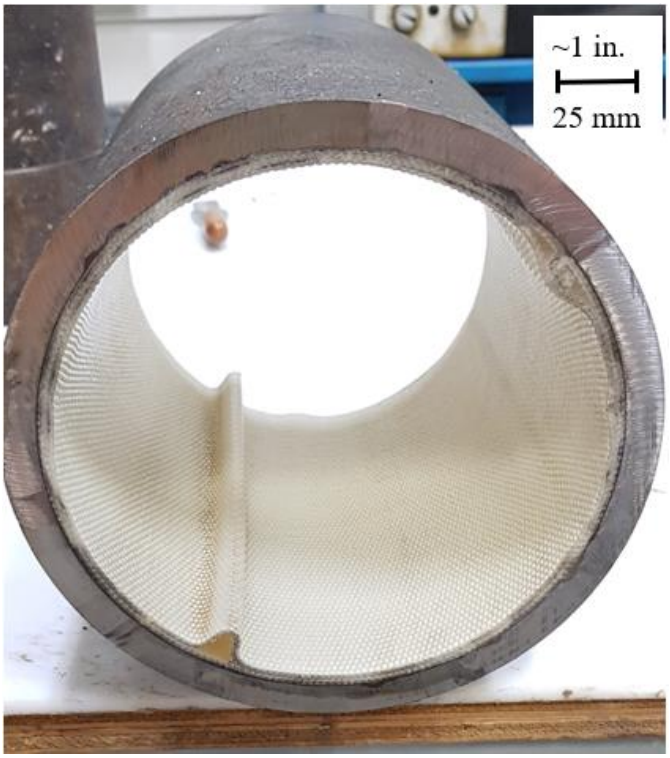

Figure 1.4. Aqua-pipe Geotextile Lining after Curing

Aqua-pipe is installed by excavating access pits as far as 985 ft (300 m) apart and pulling the lining through the pipeline between each access pit. The installation process begins by cleaning the pipe in-place. Then the lining infused with epoxy is pulled into place. Hot water or steam is run through the pipeline, curing the epoxy resin. Finally, a robot reinstates service connections from within the pipeline, and the lining is pressure-tested

There are two generations of Aqua-pipe. The first generation is being tested at Cornell, and the second generation is in development. The second generation improves on the first generation by being able to adapt to variation in host pipe diameter without creating longitudinal folds in the lining. Unless otherwise identified, the lining material referenced in this report is generation one Aqua-pipe.

Report Organization

This thesis is organized into six chapters. Chapter 1 provides report organization and introductory information on the CIPP used in this study. Chapter 2 provides stress vs. strain properties of Aqua-pipe lining determined through tensile coupon tests. Chapter 3 provides a summary of force vs displacement relationships determined through direct tension testing. Chapter 4 provides a description of special friction tests. The friction tests were performed to explore the relationship between axial resistance to movement between pipe and lining and the internal lining pressure. Chapter 5 provides the results of direct shear tests and an estimate of the coefficient of friction between lining and host pipe. Chapter 6 summarizes the test results and key findings.

CHAPTER 2

TENSILE COUPON TESTS

Introduction

This section of the report describes the uniaxial tensile coupon testing and results for the Aqua-pipe material in the warp and weft directions. The warp and weft directions pertain to the longitudinal and circumferential directions, respectively. Tensile coupon specimens were cut and machined from flat cured lining sections and tested in accordance with ASTM–D3039 2017 (ASTM, 2017) for the specimens in the warp direction. Tensile coupon specimens in the weft direction were cut and machined from flat cured lining sections and tested in accordance with ASTM-D638 2014 (ASTM, 2014).

Tensile Coupon Testing and Procedure

A Baldwin Hamilton 60 BTE Universal Testing Machine was used to apply the tensile loads. The load frame was fitted with a pressure sensor to measure axial force. Tensile strain was measured using strain gages epoxied to the specimen surface. A laser extensometer was used to measure specimen elongation. Figure 2.1 is a photograph of an Aqua-pipe specimen for the warp direction in the testing apparatus. The photograph shows axial and transverse gages on the test specimen as well as the laser extensometer strips that were used for measurements of extension with a laser beam.

Six tensile coupon specimens were tested. Three specimens were cut in the warp direction, and three specimens were cut in the weft direction. All six specimens were instrumented with axial and transverse strain gages. Schematics of the specimens in the warp and weft directions are provided in Figure 2.2 and Figure 2.3, respectively. The width of the specimens was approximately 0.15 in. (3.8 mm) in the warp direction and

0.20 in. (5.8 mm) in the weft direction. The gages were mounted in the center of the specimen. Such gages frequently debond at tensile strains of 2 to 4%. To provide supplemental measurements of strain beyond the 2-4% range, the laser extensometer was used to measure axial strain to failure. The extensometer is not as accurate as the strain gages at smaller strains, but it provides for reliable assessment of strain at larger values, specifically those beyond the initiation of plastic deformation.

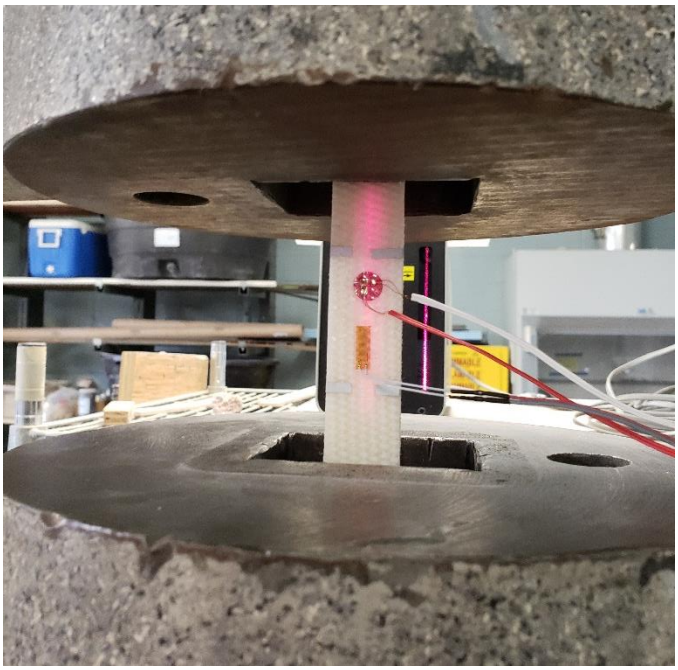

Figure 2.1. Tensile Coupon Test Setup with Aqua-pipe Material

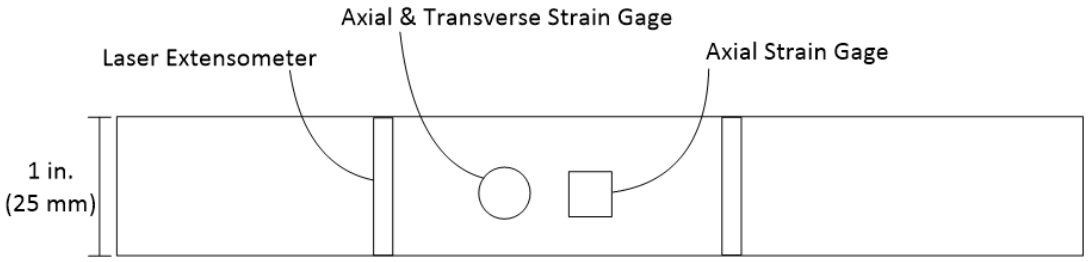

Figure 2.2. Schematic of Aqua-pipe Tensile Coupon Specimen in the Warp Direction

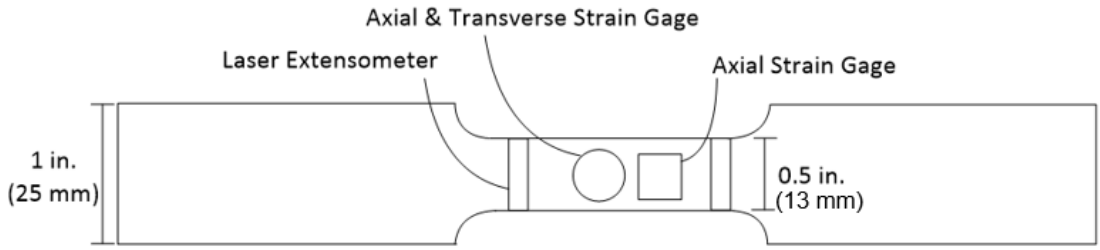

Figure 2.3. Schematic of Aqua-pipe Tensile Coupon Specimen in the Weft Direction

Stress vs. Strain Data

The stress applied throughout the uniaxial tension test was computed by dividing the measured force by the original cross-sectional area of the tensile coupon. This strain generally is referred to as engineering strain. The uniaxial stress vs. axial strain plots are shown in Figure 2.4 and Figure 2.5 for specimens in the warp and weft directions, respectively.

The results of the tensile coupon tests in each direction show good agreement. Each test was run until the woven fabric tore apart, indicating failure. Axial stress vs. strain data were used to determine the stress and strain at failure in each direction, as shown in Figure 2.4 and Figure 2.5 by the maximum measured stress. The average failure stress and strain for Specimens 1, 2, and 4 in the warp direction were 10.9 ksi and 15%, respectively, with standard deviations of 0.94 ksi and 1.2%. The average failure stress and strain for Specimens 3, 4, and 5 in the weft direction were 15.3 ksi and 11.1%, respectively, with standard deviations of 1.68 ksi and 1.6%. The ratio of the average stress at failure in the weft vs. warp direction is 1.40, which agrees closely with the ratio of stress at failure reported in Section 1.

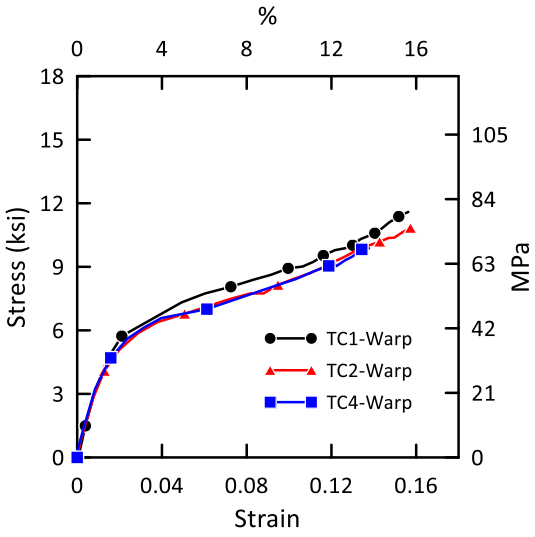

Figure 2.4. Stress vs. Strain Plots to Failure for Specimens in the Warp Direction

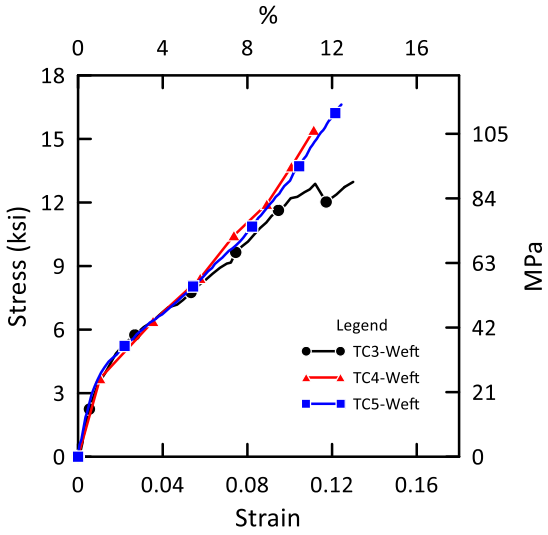

Figure 2.5. Stress vs. Strain Plots to Failure for Specimens in the Weft Direction

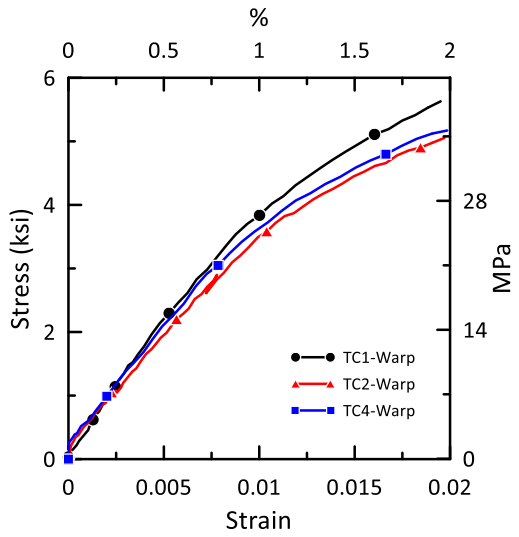

Figure 2.6. Expanded Stress vs. Strain Plots for Specimens in the Warp Direction

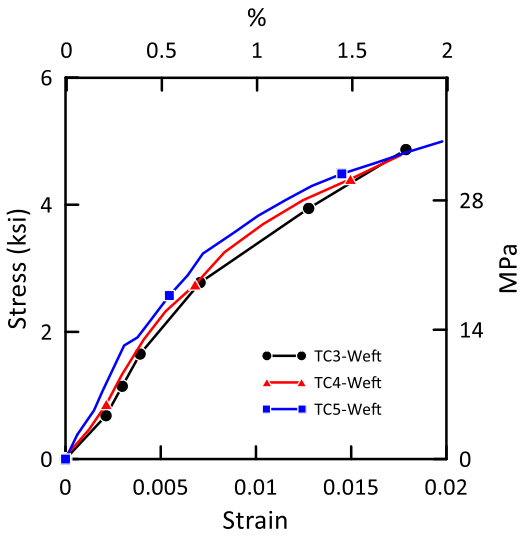

Figure 2.7. Expanded Stress vs. Strain Plots for Specimens in the Weft Direction

Expanded views of the stress vs. strain data are shown in Figure 2.6 and Figure 2.7 for the weft and warp directions, respectively. Young's modulus, E, was computed using the linear range of the stress vs. strain plots. It was determined by performing a linear

regression for stress vs. strain from 0 to approximately 0.5% strain. The average Young's modulus for Specimens 1, 2, and 4 in the warp direction is 390 ksi with a standard deviation of 60.7 ksi (0.42 MPa). The average Young's modulus for Specimens 3, 4, and 5 in the weft direction is 414 ksi (2.86 MPa) with a standard deviation of 29.0 ksi (0.20 MPa).

Poisson's ratio, ν, is the negative ratio of transverse strain to axial strain for uniaxial loading. Poisson's ratio was derived from the transverse vs. axial strain plots. As shown in Figure 2.8 and Figure 2.9, the linear range in the warp direction of the transverse vs. axial strain terminates at approximately 0.05 axial strain, beyond which axial strain accumulates at a faster rate than the transverse strain. The average Poisson's ratio for Specimens 1 and 4 in the warp direction is 0.23 with a standard deviation of 0.016. The average Poisson's ratio for Specimens 3, 4, and 5 in the weft direction is 0.25 with a standard deviation of 0.010.

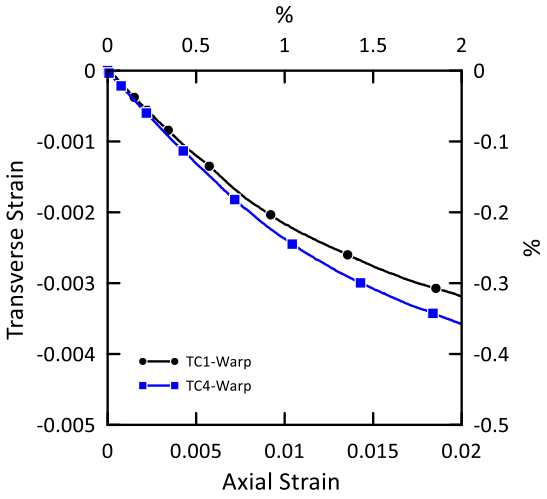

Figure 2.8. Transverse vs. Axial Strain for Tensile Stress for Specimens in the Warp Direction

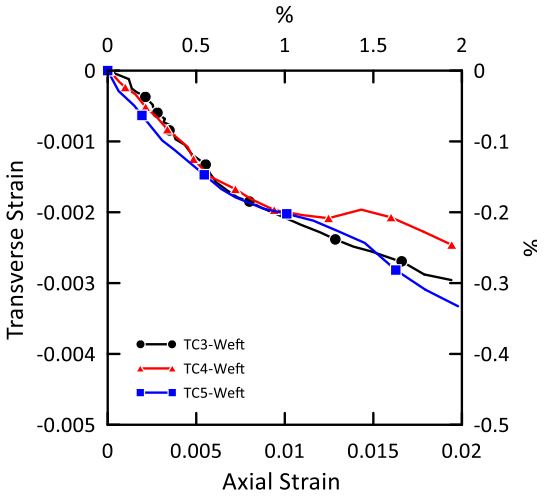

Figure 2.9. Transverse vs. Axial Strain for Tensile Stress for Specimens in the Weft Direction

Table 2.1. Summary of Material Properties from Warp Tensile Coupons

		Specimen			Average	Standard Deviation
		1	2	4		
Young's Modulus, E	ksi (GPa)	459 (3.16)	344 (2.37)	368 (2.54)	390 (2.69)	60.7 (0.42)
Poisson's Ratio, ν		0.22	N/A^1	0.25	0.23	0.016
Ultimate Tensile Strength	ksi (MPa)	11.8 (81.7)	11.0 (75.7)	10.0 (68.8)	10.9 (75.2)	0.94 (6.5)
Ultimate Tensile Strain	%	16	15	14	15	1.2

$^1N/A \quad -Not\ available$

Table 2.1 and

Table 2.2 provide summaries of the Young's modulus, tensile stress and strain at failure, and Poisson's ratio in the warp and weft directions, respectively. A close examination of the plots in Figure 2.6, Figure 2.7, Figure 2.8, and Figure 2.9 show a departure from linearity at a strain of between 0.5% and 1.0%. The Young's modulus and Poisson's ratio in both the warp and weft direction decreases at strains between 0.5% and 1.0%.

Table 2.2. Summary of Material Properties from Weft Tensile Coupons

		Specimen			Average	Standard Deviation
		3	4	5		
Young's Modulus, E	ksi (GPa)	446 (3.08)	408 (2.81)	389 (2.68)	414 (2.86)	29.0 (0.20)
Poisson's Ratio, ν		0.26	0.24	0.25	0.25	0.010
Ultimate Tensile Strength	ksi (MPa)	13.4 (92.6)	16.0 (110)	16.6 (115)	15.3 (106)	1.68 (11.6)
Ultimate Tensile Strain	%	9.3	11.5	12.5	11.1	1.6

$^1N/A \quad -Not\ available$

Lining Stress vs. Strain Response

In Figure 2.10, the stress vs. strain data for the warp and weft directions are plotted at the same scale. From zero to between 0.5% and 1.0% strain, the lining responds as a linear elastic solid. The Poisson's ratio is approximately 0.24 in both directions, and the difference in the Young's modulus is less than 7% lower in the warp than in the weft direction. In this range of tensile strain, the Young's modulus and Poisson's ratio are controlled principally by the epoxy.

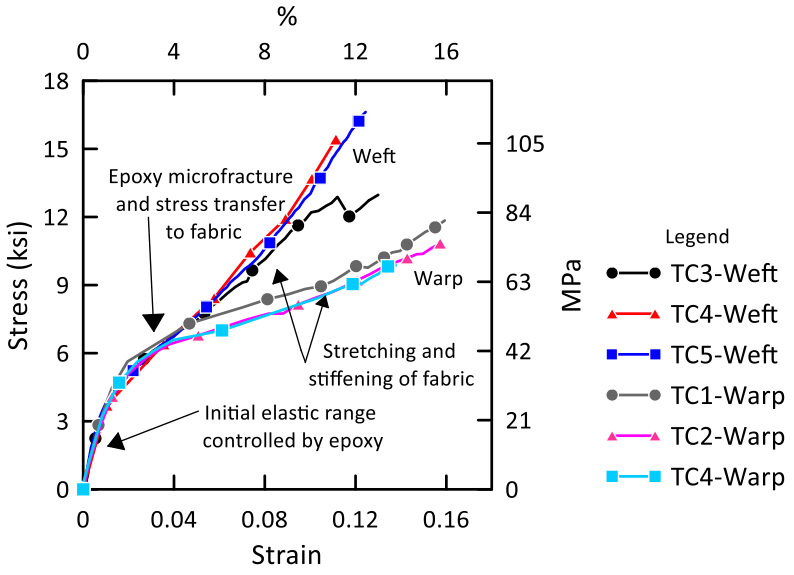

Figure 2.10. Stress vs. Strain Plots for Specimens in the Warp and Weft Directions

As the strain approaches and exceeds 1.0%, micro-fractures develop in the epoxy, and stress is transferred increasingly from the epoxy matrix to the fabric. This stress transfer results in a reduction of modulus. Moreover, the fabric stretches more in the warp direction than in the weft direction, where the strength of fibers is greater. As tensile strain exceeds approximately 5%, the fibers stretch and tighten, leading to increased modulus in both the warp and weft directions. The stiffness and strength in the weft direction exceed those in the warp direction due to the continuous nature of fibers in the weft direction.

CHAPTER 3

DIRECT TENSION TESTS

Introduction

This section summarizes the results of direct tension tests on nominal 6 in. (152 mm) diameter pipe specimens with Aqua-pipe lining. The direct tension tests were performed to evaluate the debonding characteristics between the Aqua-pipe lining and host pipe as well as determine the force vs. displacement response of the lined pipe.

A summary of the full-scale direct tension tests performed as part of this investigation is provided in Table 3.1 that includes internal pressure, test pipe specimen length, load frame, sampling rate, and whether the pipe was new or old. Seven tests were performed and are labeled DT1 through DT7. The first four direct tension tests were performed on new ductile iron (DI) pipe that was procured directly from a local DI pipe supplier. The remaining tests were performed on older cast iron (CI) pipe that was excavated and removed from the field. All tests were loaded at a displacement rate of 1 in./min (25.4 mm/min).

Direct Tension Test Setup

Figure 3.1 and Figure 3.2 show plan views of the axial tension test setup and equipment for large and small load frames. An actuator, load cell, and load frame were used to apply tensile load to the test specimen in each setup. The test specimens consisted of nominal 6 in. (152 mm) diameter DI and CI pipes lined with Aqua-pipe that was installed by Sanexen. The specimen lengths were 8.5 ft (2.6 m) or 17 ft (5.2 m). Each specimen was fitted with end caps to allow for internal pressurization during loading. A photo of the test setup using the large load frame is shown in Figure 3.3, and a photo of the test setup using the small load frame is shown in Figure 3.4. Each test specimen

consisted of two pipe sections of equal length on each side of a gap, representing a round crack.

In the small load frame setup, an actuator and load cell were installed at the south end of the load frame to apply and measure tensile force, respectively. The load cell had a capacity of 110 kips (489 kN) in the small and large load frame setups. In the large load frame setup, an actuator and load cell were installed at the north end of the load frame to apply and measure tensile force, respectively.

The actuator in DT1 had a tensile load capacity of 55 kips (245 kN) and stroke of 6 in. (150 mm). For DT2 through DT7, the actuator had a tensile load capacity of 63 kips (280 kN) and stroke of 6 ft (1.83 m). A series of three wedge action restraints were used at either end of each specimen to transfer load from the actuator and loading frame to the specimen. The three restraining collars acted as a grip for the pipes during axial load application.

Two electronic pressure transducers, located at the end cap and water source, measured internal water pressure during the test sequence when internal pressure was applied. String potentiometers (string pots) were attached to the specimen and restraints to measure axial displacements along the specimen.

Axial and circumferential strain gages were located on the exterior surface of the pipe specimen at varying distances from the gap at the center of the specimen. The gages were applied at the 12, 3, 6, and 9 o´clock positions around the pipe (crown, east springline, invert, and west springline, respectively). A detailed list of the instrumentation is provided for each test under Instrumentation and Experimental Results.

Table 3.1. Summary of Direct Tension Tests

Test	Pipe Condition	Length ft (m)	Pressure psi (kPa)	Sampling Rate Hz
Direct Tension 1 (DT1)	New DI	17 (5.2)	0	50
Direct Tension 2 (DT2)	New DI	8.5 (2.6)	0	20
Direct Tension 3 (DT3)	New DI	8.5 (2.6)	80 (551)	20
Direct Tension 4 (DT4)	New DI	17 (5.2)	0	2
Direct Tension 5 (DT5)	Field CI	8.5 (2.6)	80 (551)	2
Direct Tension 6 (DT6)	Field CI	8.5 (2.6)	80 (551)	25
Direct Tension 7 (DT7)	Field CI	16 (4.9)	80 (551)	50

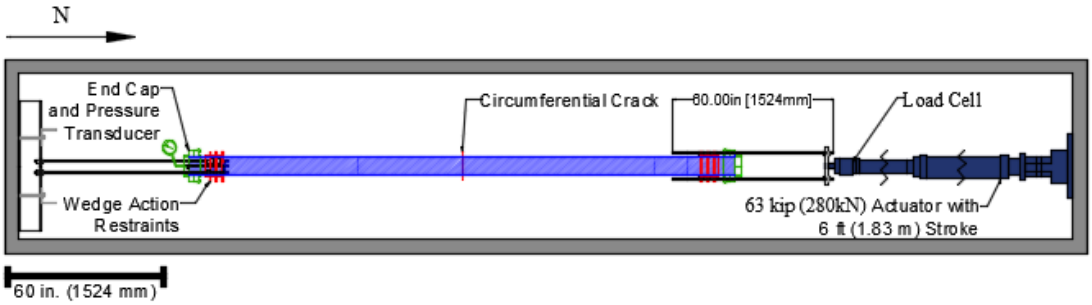

Figure 3.1. Plan View of a Direct Tension Test in the Large Load Frame

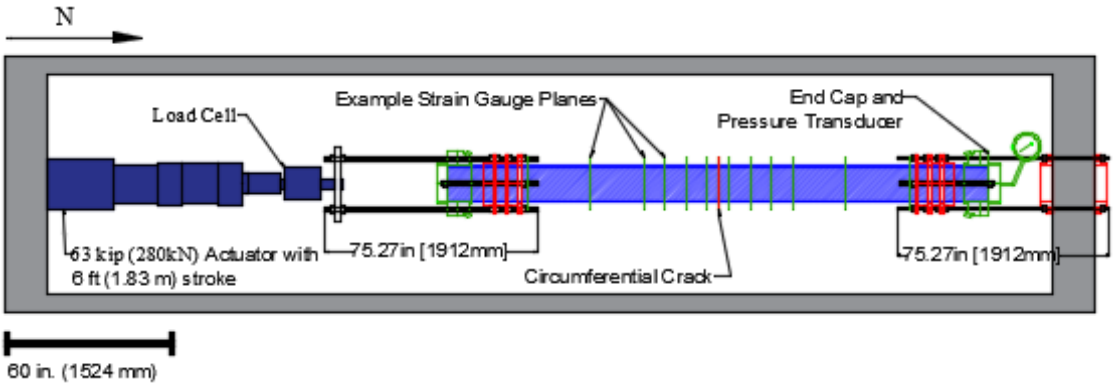

Figure 3.2. Plan View of a Direct Tension Test in the Small Load Frame

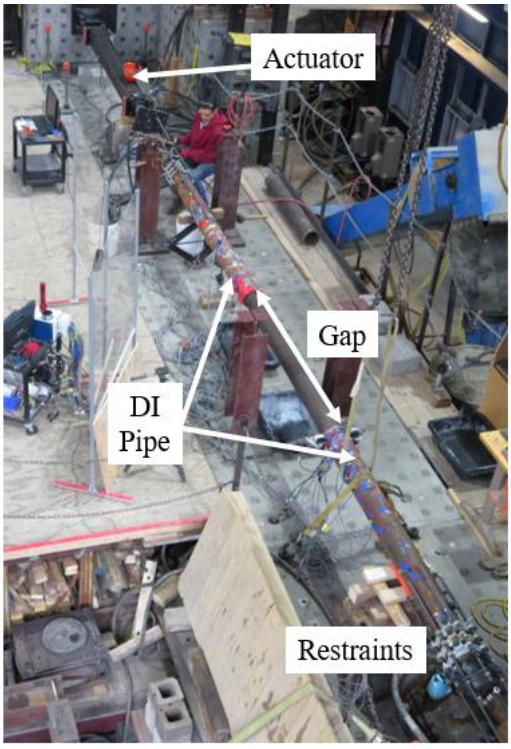

Figure 3.3. Large Load Frame (Facing North)

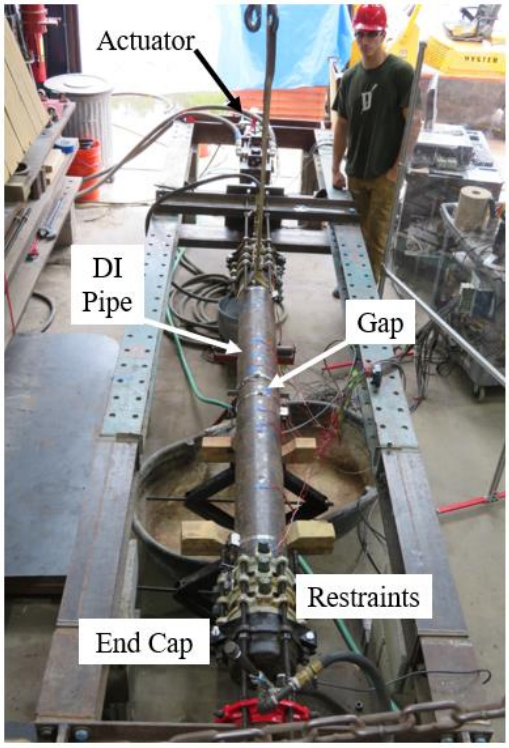

Figure 3.4. Small Load Frame (Facing South)

Test Specimen Preparation

The test specimens for direct tension tests DT1, DT2, DT3, and DT4 were prepared by Sanexen using commercially available DI pipe without an internal cement lining. The installation procedure was the same as used under field conditions, except that the interior pipe surface was not aged and thus did not require cleaning before placement of the lining. The DI pipe without cement mortar lining had a clean, new interior surface that mobilized the maximum interface friction between the host pipe and the Aqua-pipe lining.

To prepare test specimens with interior surfaces representative of pipelines in the field, the test specimens for direct tension tests DT5, DT6, and DT7 were taken from CI pipelines, which had operated in the field for many years. These specimens were cleaned

by Sanexen following their standard field installation procedures. The lining-pipe interface condition for DT5, DT6, and DT7 are more representative of field conditions than the pipes used in tests DT1 through DT4. The interface friction between the host pipe and Aqua-pipe lining in the field samples was significantly lower than that of the pipe specimens with new interior surfaces for the first-time movement of the lining along the pipe. The characterization of the interface between DI and CI pipe and the lining before and after repeated loading are detailed in Chapter 5 Direct Shear Tests.

Before lining a test specimen, a gap, approximately 0.25 in. (6 mm) wide, was located at the center of the specimen to replicate a round crack or gap between spigot and bell in an aging, deteriorated joint. DI pipe was used as a proxy for CI pipe. Both DI and CI pipes have similar metallurgical surface characteristics and roughness, as well as frictional and bonding properties.

Test Sequence

After the specimen was instrumented and centered in the test frame, the test sequence was initiated by starting the data acquisition system and laboratory hydraulic systems. The loading restraints at either end of the specimen were tightened to avoid end movement due to pressurization. The pipe was pressurized next with an internal water pressure of 80 psi (551 kPa). The tests were performed under displacement control using the servo-hydraulic actuator at the end of the test frame. The actuator was located at the south end for tests in the small load frame and at the north end in the large load frame.

During the application of axial load, the Aqua-pipe lining separated itself, or debonded, from the DI host pipe starting at the centerline and then progressing towards the north and/or south ends. As the debonding front reached each strain gage station, there was a rapid reduction in strain in the DI pipe. As the Aqua-pipe lining debonded in the north or south direction completely, displacement was applied until the specimen was no

longer capable of holding internal water pressure or until it reached the extent of the actuator range. The pipe on the debonded side of the specimen center was pulled from the lining in select tests.

Instrumentation and Experimental Results

The following subsections provide the instrumentation plan and key experimental results from the seven direct tension tests. The axial force vs. crack opening, influence of internal pressure, geometric pipe effects, and debonding trends are described and compared in these sections.

DT1

As indicated in Table 3.1, DT1 was performed with a 17-ft (5.2 m)-long specimen in the large load frame. It was tested with zero internal pressure at a sampling rate of 50 Hz.

Table 3.2 provides a list of the instrumentation used in DT1. The instrumentation for DT1 involved strain gages applied at 11 different locations both south and north of the gap. Longitudinal strain gages at the crown and invert were established at seven locations to 20 in. (508 mm) south and north of the gap. Circumferential strain gages at the crown and invert were positioned at 4 in. (102 mm) and 10 in. (254 mm) south and north of the center of the pipe. Only longitudinal gages at the crown were placed at distances greater than 20 in. (508 mm) from the pipe center. Horizontal string pots were located at eight different locations to measure the opening of the center gap as well as slip of the restraints.

Figure 3.5 (a) – (d) show photographs of the DT1 test pipe. Figure 3.5 (a) shows the pipe at the beginning of the test. Strain gages on the crown of the pipe and a string pot along the eastern springline of the pipe can be seen in the photo. Figure 3.5 (b) – (c)

show the pipe after the first and second 6 in. (152 mm) of actuator displacement. Figure 3.5 (d) shows the maximum 12 in. (305-mm) opening of the center crack near the end of the test. At 12 in. (305 mm) of crack opening, the geometric limits of the loading frame were met, and the specimen was unloaded.

Figure 3.6 shows the axial force vs gap, or crack, opening. As displacement was applied, the axial load increased rapidly so that the slope of the plot appears to be a vertical line. After approximately 1 in. (25 mm) of crack opening, the test was paused, causing the first cyclic loading in the figure.

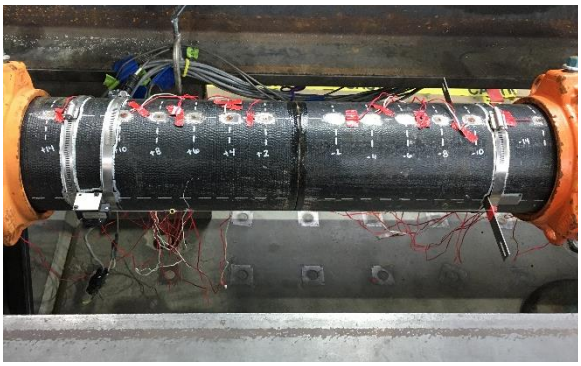

a) View of DT1 Specimen in Load Frame before Test Initiation

(b) View of Lining Exposed after First 6 in. (152 mm) of Actuator Displacement

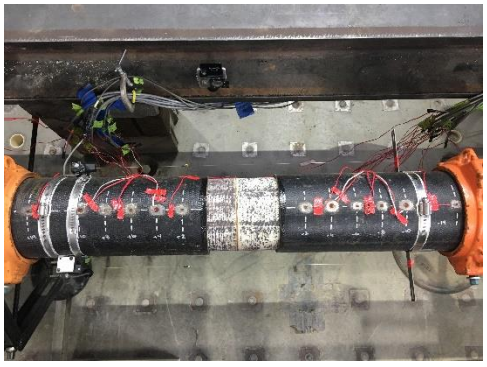

c) View of Lining Exposed after Second 6 in. (152 mm) of Actuator Displacement

d) View of Lining Exposed after Completion of Actuator Displacement

Figure 3.5. Photos of the Center Gap at Various Levels of Displacement during DT1

Table 3.2. Instrumentation List for DT1

Location	Instrument Description	Local Instrument Name
66 in. South of Centerline	Crown, Axial Strain	-66C
54 in. South of Centerline		-54C
42 in. South of Centerline		-42C
30 in. South of Centerline		-30C
20 in. South of Centerline		-20C
	Invert, Axial Strain	-20I
14 in. South of Centerline	Crown, Axial Strain	-14C
	Invert, Axial Strain	-14I
10 in. South of Centerline	Crown, Axial Strain	-10C
	Crown, Circumferential Strain	-10CC
	Invert, Axial Strain	-10I
	Invert, Circumferential Strain	-10IC
8 in. South of Centerline	Crown, Axial Strain	-8C
	Invert, Axial Strain	-8I
6 in. South of Centerline	Crown, Axial Strain	-6C
	Invert, Axial Strain	-6I
4 in. South of Centerline	Crown, Axial Strain	-4C
	Crown, Circumferential Strain	-4CC
	Invert, Axial Strain	-4I
	Invert, Circumferential Strain	-4IC
2 in. South of Centerline	Crown, Axial Strain	-2C
	Invert, Axial Strain	-2I
2 in. North of Centerline	Crown, Axial Strain	2C
	Invert, Axial Strain	2I
4 in. North of Centerline	Crown, Axial Strain	4C
	Crown, Circumferential Strain	4CC
	Invert, Axial Strain	4I
	Invert, Circumferential Strain	4IC
6 in. North of Centerline	Crown, Axial Strain	6C
	Invert, Axial Strain	6I
8 in. North of Centerline	Crown, Axial Strain	8C
	Invert, Axial Strain	8I
10 in. North of Centerline	Crown, Axial Strain	10C
	Crown, Circumferential Strain	10CC
	Invert, Axial Strain	10I
	Invert, Circumferential Strain	10IC
14 in. North of Centerline	Crown, Axial Strain	14C
	Invert, Axial Strain	14I
20 in. North of Centerline	Crown, Axial Strain	20C
	Invert, Axial Strain	20I

Table 3.2. Instrumentation List for DT1

Location	Instrument Description	Local Instrument Name
30 in. North of Centerline	Crown, Axial Strain	30C
42 in. North of Centerline	Crown, Axial Strain	42C
54 in. North of Centerline	Crown, Axial Strain	54C
66 in. North of Centerline	Crown, Axial Strain	66C
Centerline	Horizontal String Pot	N-Pipe
		N-Liner
		S-Pipe
		S-Liner
		HSP_East
		HSP_West
Restraining Collars, North of Centerline		N_Slip
Restraining Collars, South of Centerline		S_Slip
Actuator, South of Centerline	Actuator Displacement	Act-Disp

1 in. = 25.4 mm

After resuming the test, multiple load reload cycles were applied until a maximum gap opening of 12 in. (305 mm) was achieved. Six unloading and loading cycles are shown in the figure, which reflect multiple adjustments in the 6 in. (152 mm) stroke actuator to develop large axial displacement of the pipe relative to the lining.

The maximum axial force recorded varied between 26 kips (116 kN) and 29 kips (129 kN). This force represents the debonding capacity of the lining, which is the force required to propagate a Type II fracture between the lining and inside surface of the pipe (Argyrou et al, 2018). The maximum debonding force varied roughly ± 5% along the pipe specimen, with an average of approximately 27.5 kips (122 kN).

Additional insight with respect to the debonding characteristics of the lining can be obtained from the strain gage readings. Figure 3.7 shows plots of the crown and invert strains measured by longitudinal strain gages, 6C and 6I, at 6 in. (152 mm) north of the

pipe specimen center. Each minimum reading indicates when debonding of the lining had fully propagated to the location of the gage. At approximately 1.7 in. (43 mm) of gap opening, the invert strain dropped to its minimum value, followed by the crown strain that dropped to its minimal value at 1.9 in. (48 mm) of gap opening. There is a lag of approximately 0.20 – 0.25 in. (5.1 – 6.4 mm) between the minimum readings.

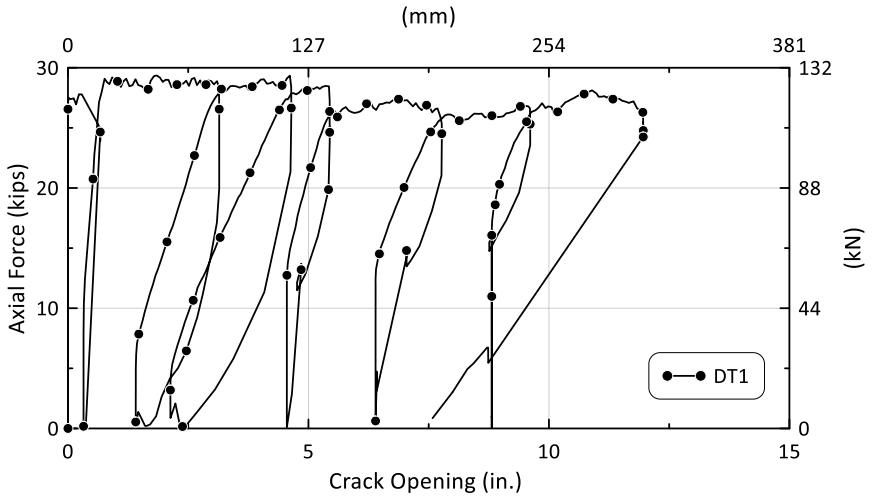

Figure 3.6. Axial Force vs. Crack Opening for DT1

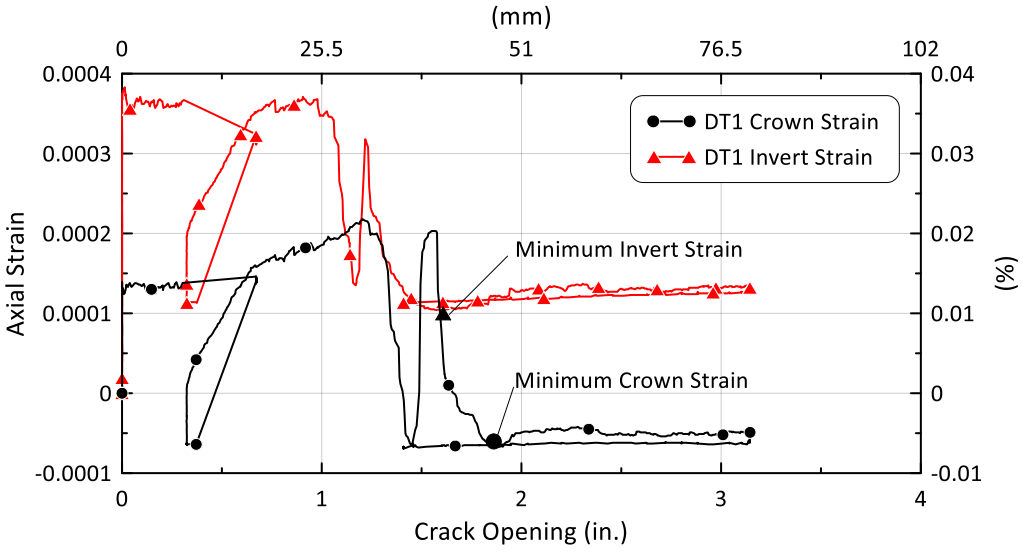

Figure 3.7. Longitudinal Strain at Strain Gage Station 6 vs Crack Opening for DT1 Specimen

DT2

As indicated in Table 3.1, DT2 was performed with an 8.5-ft (2.6 m)-long specimen in the small load frame. It was tested with no internal pressure at a sampling rate of 20 Hz. The test consisted of two stages. The first stage included the propagation of the debonding front along the pipe, and the second stage included pulling the DI pipe off the Aqua-pipe lining.

Table 3.3 provides a list of the instrumentation used in DT2. The instrumentation for DT2 involved strain gages applied at 10 different locations both south and north of the gap at the center of the test pipe. Longitudinal strain gages at the crown and invert were established at six locations to 16 in. (406 mm) south and north of the gap. Longitudinal strain gages at the crown, invert, east springline, and west springline were positioned at 4 in. (102 mm) and 6 in. (152 mm) south and north of the center of the pipe. Only longitudinal gages at the crown were placed at distances greater than 16 in. (406 mm) from the pipe center. Horizontal string pots were located at six different locations to measure opening of the center gap as well as any slip of the restraints.

Figure 3.8 (a) - (b) show photographs of the DT2 specimen after the lining fully debonded from the DI host pipe. Figure 3.8 (a) shows the specimen in the small load frame. A string pot on the crown of the crack opening and several strain gages are visible in Figure 3.8 (b).

The actuator displacement and crack opening vs. time are shown in Figure 3.9. Actuator displacement is a direct measurement of the hydraulic piston movement. Crack opening represents the relative movement between the north and south pipe lengths. Only the south section of the pipe specimen debonded from the lining so the gap opening is equivalent to pipe movement along the south part of the lining.

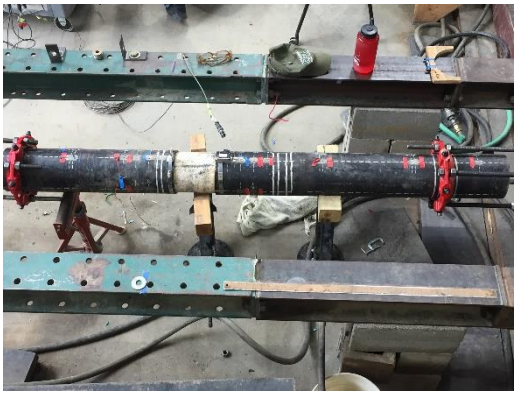

a) Full View of DT2 Specimen in Load Frame

(b) View of Lining Exposed After DT2

Figure 3.8. Photos of the Center Gap at the End of DT2

Crack opening was determined by averaging the displacements of the horizontal string pots, N-Pipe and S-Pipe, across the centerline. At approximately 1 min, there was a slip of the retaining collars that resulted in an offset between the actuator displacement and gap opening. Further crack opening occurred in unison with the actuator displacement, indicating no further slip of the restraining collars and no significant axial deformation of the DI pipe.

As described previously, the test consisted of propagating the debonding front along the entire south pipe section, followed by pulling the debonded side of the DI pipe off the Aqua-pipe lining. After the maximum range of the string pot was exceeded, further crack opening was measured by the actuator.

Figure 3.10 shows the axial force vs. crack opening until 12.5 in. (318 mm) of crack opening. Both the debonding and pull-off phases of the test are identified. A maximum force of approximately 27 (120 kN) kips was reached at a corresponding crack opening of 5.5 in. (140 mm). At that point, the debonding front reached the south end of the pipe with a corresponding rapid decrease in axial load. The test was paused before the second phase of loading.

Table 3.3. Instrumentation List for DT2

Location	Instrument Description	Local Instrument Name
40 in. South of Centerline	Crown, Axial Strain	-40C
30.5 in. South of Centerline		-30_5C
30 in. South of Centerline		-30C
16.5 in. South of Centerline		-16_5C
16 in. South of Centerline		-16C
	Invert, Axial Strain	-16I
8 in. South of Centerline	Crown, Axial Strain	-8C
	Invert, Axial Strain	-8I
6 in. South of Centerline	Crown, Axial Strain	-6C
	Invert, Axial Strain	-6I
	East, Axial Strain	-6E
	West, Axial Strain	-6W
4 in. South of Centerline	Crown, Axial Strain	-4C
	Invert, Axial Strain	-4I
	East, Axial Strain	-4E
	West, Axial Strain	-4W
3 in. South of Centerline	Crown, Axial Strain	-3C
	Invert, Axial Strain	-3I
2 in. South of Centerline	Crown, Axial Strain	-2C
	Invert, Axial Strain	-2I
2 in. North of Centerline	Crown, Axial Strain	2C
	Invert, Axial Strain	2I
3 in. North of Centerline	Crown, Axial Strain	3C
	Invert, Axial Strain	3I
4 in. North of Centerline	Crown, Axial Strain	4C
	Invert, Axial Strain	4I
	East, Axial Strain	4E
	West, Axial Strain	4W
6 in. North of Centerline	Crown, Axial Strain	6C
	Invert, Axial Strain	6I
	East, Axial Strain	6E
	West, Axial Strain	6W
8 in. North of Centerline	Crown, Axial Strain	8C
	Invert, Axial Strain	8I
16 in. North of Centerline	Crown, Axial Strain	16C
	Invert, Axial Strain	16I
16.5 in. North of Centerline	Crown, Axial Strain	16_5C
30 in. North of Centerline		30C
30.5 in. North of Centerline		30_5C
40 in. North of Centerline		40C

Table 3.3. Instrumentation List for DT2

Location	Instrument Description	Local Instrument Name
Centerline	Horizontal String Pot	N Pipe
		S Pipe
Centerline	Horizontal String Pot	HSP_East
		HSP_West
Restraining Collars, North of Centerline		N_Slip
Restraining Collars, South of Centerline		S_Slip
Actuator, South of Centerline	Actuator Displacement	SP_Act_Disp
Actuator, South of Centerline	Actuator Displacement	Act-Disp

1 in. = 25.4 mm

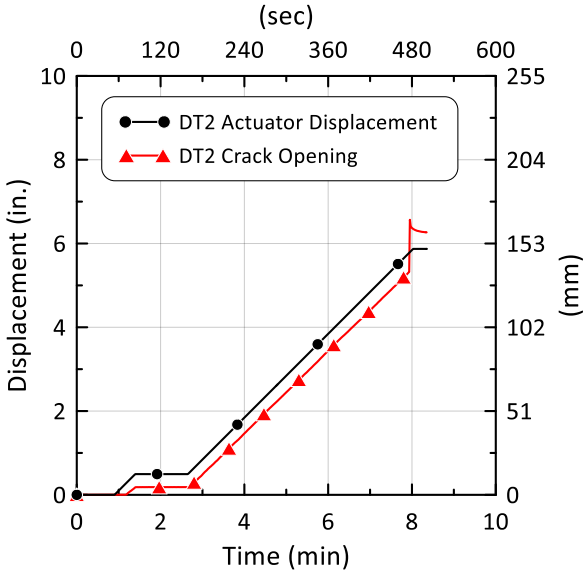

Figure 3.9. Actuator Displacement and Crack Opening vs. Time for DT2 Specimen

As explained with respect to DT1, the strain gage measurements show when the debonding front reaches each gage station. By correlating the string pot measurements of average gap opening in DT2 with debonding front propagation to gage stations at increasing distances from the specimen center, one can plot the debonding length as a

function of gap opening as shown in Figure 3.11. As explained previously, the debonding occurred in the south pipe section so that the gap opening is equivalent to the relative axial displacement between the initial center gap location and south section of pipe.

As shown in Figure 3.11, the debonding front propagated rapidly through the south section of pipe to 40 in. (1016 mm) at a gap opening of 0.5 in. (13 mm). Further debonding was affected by additional axial resistance as the southern section of the pipe was pulled along the lining. The increase in debonding length after 40 in. (1016 mm) is presented as a dashed line to indicate that there is uncertainty about the relationship between debonded length and crack opening from 40 to 51 in. (1016 to 1295 mm). The displacements after the initial gap opening of 0.5 in. (13 mm) and a corresponding 40 in. (1016 mm) of debonding correlate with a steady rise in axial force from approximately 20 kips (89 kN) to 27 kips (120 kN) as shown in Figure 3.10.

The second phase of the test consisted of pulling and pushing the DI pipe over the south section of the Aqua-pipe lining. Figure 3.10 shows the first iteration of pulling the south section of pipe along the lining. The force increased to 1.5 kips (6.7 kN) rapidly and decreased to zero as the pipe moved towards the end of the lining.

Figure 3.12 shows the axial force vs. crack opening for the initial pipe pull-off as well as two additional cycles of pushing and pulling the DI pipe along the lining. When the pipe was being pulled from the lining, it was in tension (positive force). The lining was in compression (negative force) while the pipe was pushed onto it. The axial force initially increased at the beginning of pipe pull off and decreased to zero. When the pipe was pushed back onto the lining, the force increased slowly from zero to the initial force necessary to pull the pipe off.

Figure 3.13 shows the average outside lining diameter plotted with respect to distance along the south side of the lining that was exposed after the south section of the pipe was pulled from the lining. The diameter is measured from the center of the specimen at zero to near the south end of the lining at 48 in. (1219 mm).

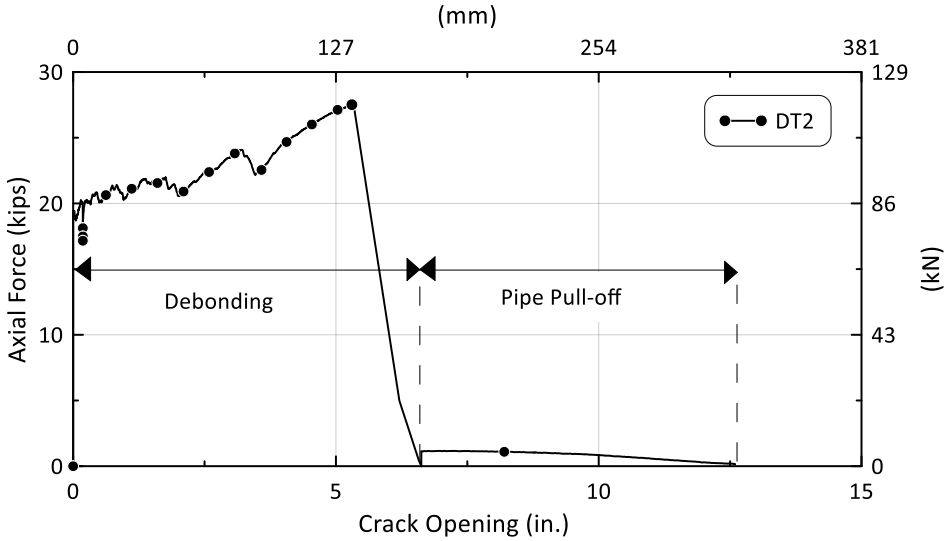

Figure 3.10. Axial Force vs. Crack Opening for the DT2 Specimen

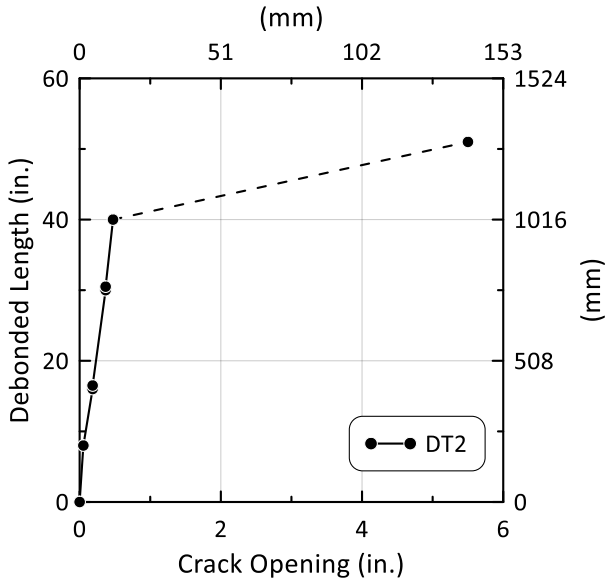

Figure 3.11. Location of Debonding Front vs. Crack Opening of the DT2 Specimen

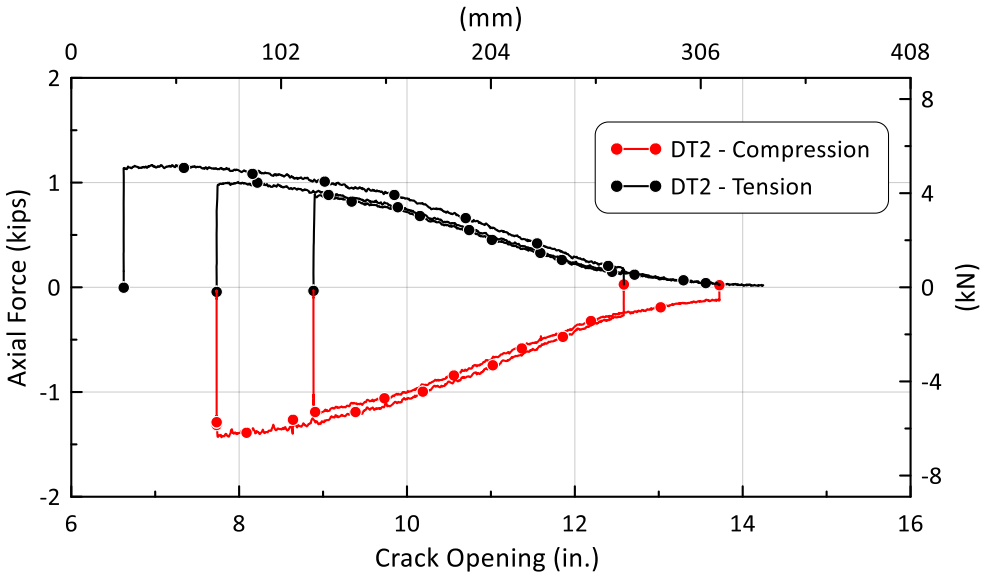

Figure 3.12. Axial Force vs. Crack Opening During Pipe Pull-off

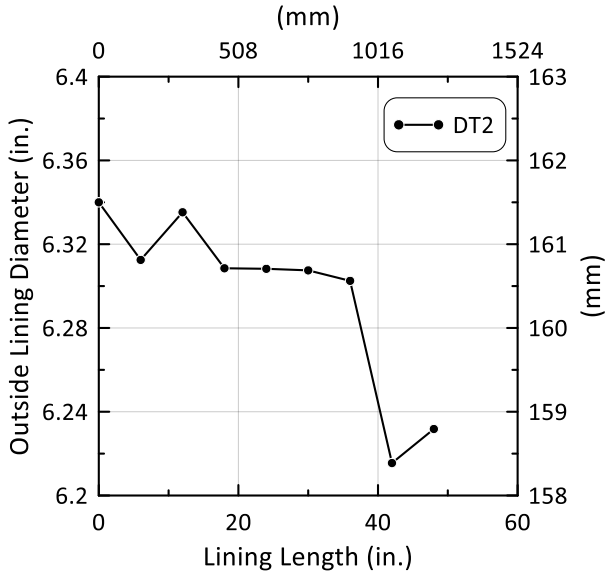

Figure 3.13. Average Outer Diameter of Lining Along the South Section of the DT2 Specimen

Because the lining was cast and cured inside the pipe, the outside diameter of the lining is the inside diameter of the pipe. As the pipe was pulled along the lining, the larger end of the pipe was pulled across a lining diameter that decreased until a minimum diameter at about 42 in. (1067 mm) south of the initial center gap. Because the end of the pipe was displaced past a lining diameter lower than that of the pipe, contact between the inside diameter of the pipe and outside diameter of the lining was lost with a corresponding loss of shear resistance between the two surfaces. This geometric condition resulted in the reduction of axial load with increasing pipe/lining movement under tension as well as an increasing axial load with increasing pipe/lining movement under compression.

DT3

As indicated in Table 3.1, DT3 was performed with an 8.5-ft (2.6 m)-long specimen in the small load frame. It was tested with 80 psi (551 kPa) internal pressure at a sampling rate of 20 Hz.

Table 3.4 provides a list of the instrumentation used in DT3. The instrumentation for DT3 involved strain gages applied at 10 different locations both north and south of the crack at the center of the test pipe. Longitudinal strain gages at the crown and invert were established at six locations to 16 in. (406 mm) south and north of the gap. Longitudinal strain gages at the crown, invert, east springline, and west springline were positioned at 4 in. (102 mm) and 6 in. (152 mm) south and north of the center of the pipe. Only longitudinal gages at the crown were placed at distances greater than 16 in. (406 mm) from the pipe center. Horizontal string pots were located at four different locations to measure crack opening as well as any slip of the restraints. Pressure transducers were located at the end cap and water source to monitor the internal pressure.

Table 3.4. Instrumentation List for DT3

Location	Instrument Description	Local Instrument Name
40 in. South of Centerline	Crown, Axial Strain	-40C
30.5 in. South of Centerline		-30_5C
30 in. South of Centerline		-30C
16.5 in. South of Centerline		-16_5C
16 in. South of Centerline		-16C
	Invert, Axial Strain	-16I
8 in. South of Centerline	Crown, Axial Strain	-8C
	Invert, Axial Strain	-8I
6 in. South of Centerline	Crown, Axial Strain	-6C
	Invert, Axial Strain	-6I
	East, Axial Strain	-6E
	West, Axial Strain	-6W
4 in. South of Centerline	Crown, Axial Strain	-4C
	Invert, Axial Strain	-4I
	East, Axial Strain	-4E
	West, Axial Strain	-4W
3 in. South of Centerline	Crown, Axial Strain	-3C
	Invert, Axial Strain	-3I
2 in. South of Centerline	Crown, Axial Strain	-2C
	Invert, Axial Strain	-2I
2 in. North of Centerline	Crown, Axial Strain	2C
	Invert, Axial Strain	2I
3 in. North of Centerline	Crown, Axial Strain	3C
	Invert, Axial Strain	3I
4 in. North of Centerline	Crown, Axial Strain	4C
	Invert, Axial Strain	4I
	East, Axial Strain	4E
	West, Axial Strain	4W
6 in. North of Centerline	Crown, Axial Strain	6C
	Invert, Axial Strain	6I
	East, Axial Strain	6E
	West, Axial Strain	6W
8 in. North of Centerline	Crown, Axial Strain	8C
	Invert, Axial Strain	8I
16 in. North of Centerline	Crown, Axial Strain	16C
	Invert, Axial Strain	16I
16.5 in. North of Centerline	Crown, Axial Strain	16_5C
30 in. North of Centerline		30C
30.5 in. North of Centerline		30_5C
40 in. North of Centerline		40C
Centerline	Horizontal String Pot	HSP_Crown

Table 3.4. Instrumentation List for DT3

Location	Instrument Description	Local Instrument Name
Centerline	Horizontal String Pot	HSP_Invert
Restraining Collars, North of Centerline	Horizontal String Pot	N_Slip
Restraining Collars, South of Centerline		S_Slip
South End Cap	Pressure Transducer	Pressure_End_cap
Water Source on Deck		Pressure_Deck
Actuator, South of Centerline	Actuator Displacement	Act-Disp

1 in. = 25.4 mm

Figure 3.14 (a) - (b) show photographs of the DT3 specimen before the start of the test and after the Aqua-pipe lining failed. At approximately 2.5 in. (64 mm) of crack opening, the liner broke in tension rather than debonding along the length of the pipe. As the DI pipe was a new, clean specimen there was a relatively large amount of frictional resistance against debonding compared to the frictional resistance mobilized in field specimens.

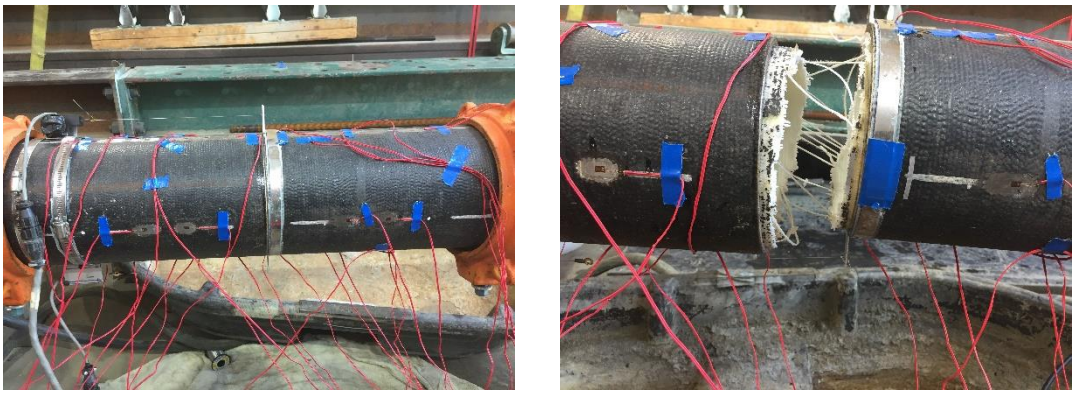

a) Full View of Specimen in Load Frame (b) View of Aqua-pipe Failure

Figure 3.14. Photos of the Center Gap at the beginning and end of DT3

Figure 3.15 shows the axial force vs. crack opening. The force increased until a maximum force of approximately 30 kips (133 kN) was reached and the Aqua-pipe lining failed at approximately 2 in. (51 mm) of crack opening. The stress at failure in

DT3 was 10.7 ksi (74 MPa). This agrees with the findings of the tensile coupon test, which show an average failure stress in the warp direction of 10.9 ksi (75 MPa).

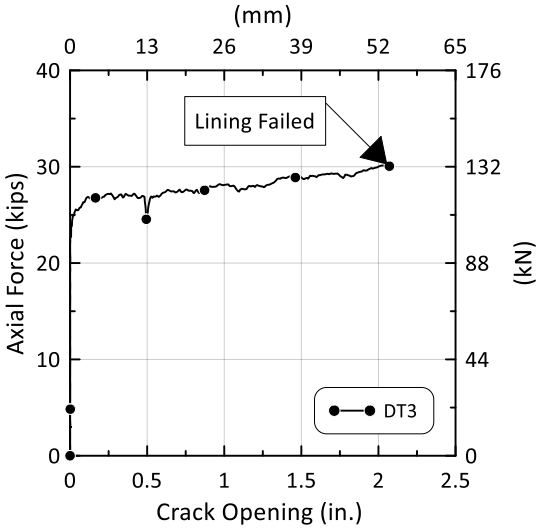

Figure 3.15. Axial Force vs. Crack Opening for DT3

DT4

As indicated in Table 3.1, DT4 was performed with a 17-ft (5.2 m)-long specimen in the large load frame. It was tested with no internal pressure at a sampling rate of 2 Hz. This specimen was later used in the friction tests described in Chapter 4.

Similar to DT2, DT4 included two phases. The first phase consisted of propagating the debonding front along the entire north pipe section. The second phase consisted of pulling the debonded side of the DI pipe, which resulted from movement of the north pipe section relative to the lining. After the maximum range of the string pot was exceeded, further crack opening was measured by the actuator.

Table 3.5 provides a list of the instrumentation used in DT4. The instrumentation for DT4 involved horizontal string pots at three different locations to measure the opening

of the center gap as well as any slip of the restraints. No strain data were recorded during DT4.

Figure 3.16 shows the axial force vs. crack opening until 20 in. (508 mm) of movement. The gap opening was caused by displacement of the north pipe section relative to the lining. Thus, the gap opening is equivalent to the axial displacement of the north pipe. The force increased rapidly at first followed by a relatively constant load of 25 kips (111 kN) until a peak load of 26.9 kips (120 kN). At about 12 in. (305 mm) of gap opening, the load dropped rapidly to 0 kips. With further crack opening the axial force began to increase.

Figure 3.17 shows the axial force vs. crack opening until 103 in. (2616 mm) when the north pipe section was pulled completely from the lining. After the sudden drop in axial force at 12 in. (305 mm) of crack opening, the force increased steadily to a maximum force of 15.5 kips (69 kN) at about 48 in. (1219 mm) of crack opening. This increase in axial force was accompanied by a cyclic loading generated as the north section of the pipe was pulled along the lining. These cycles of axial force are shown in the force vs. crack opening plot. The greatest difference between maximum and minimum load in a load cycle occurred when the maximum force of 15.5 kips (69 kN) was measured at 48 in. (1219 mm) of gap opening.

To understand the reason for the increase in cyclic as well as maximum axial force after debonding, the lining diameter was measured at various distances along the lining. Figure 3.18 shows the average outside lining diameter plotted with respect to distance along the north side of the lining that was exposed after the north section of the pipe was pulled from the lining. The diameter was measured from the center of the specimen at 0 to the north end of the lining at 104 in. (2642 mm).

Table 3.5. Instrumentation List for DT4

Location	Instrument Description	Local Instrument Name
Centerline	Horizontal String Pot	Opening Disp
Restraining Collars, North of Centerline		North Slip
Restraining Collars, South of Centerline		South Slip
Actuator, South of Centerline	Actuator Displacement	LSA1-Disp

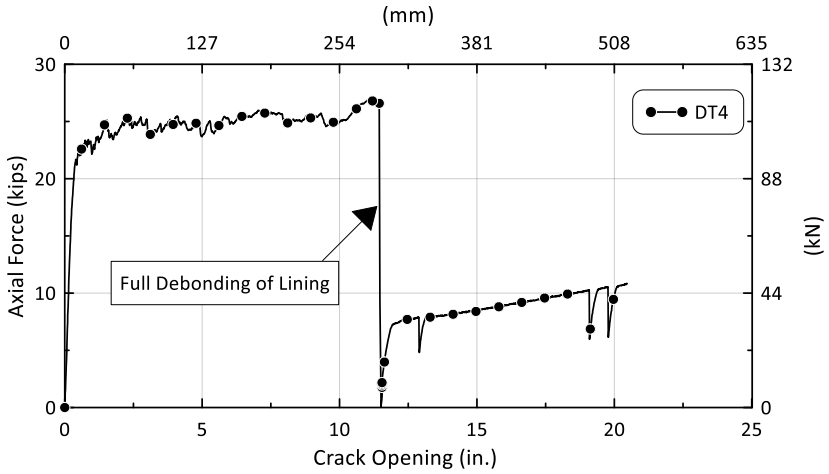

Figure 3.16. Axial Force vs. Displacement for DT4 During Debonding

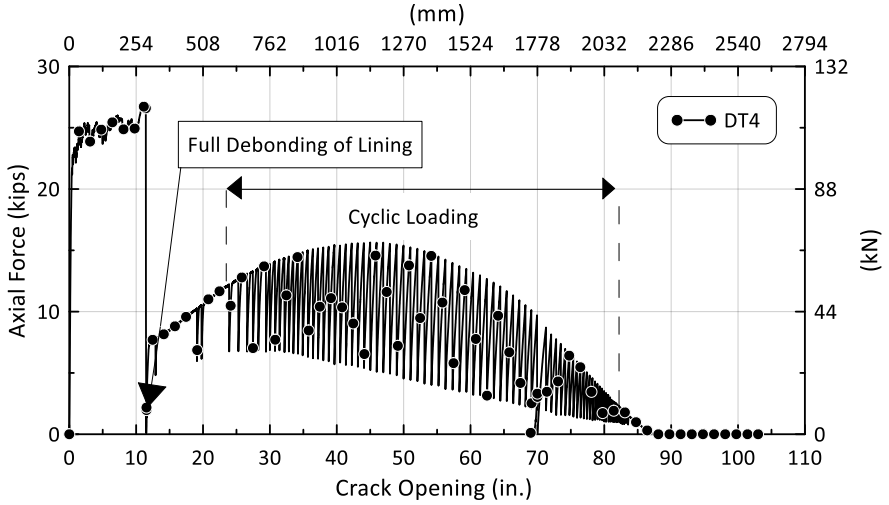

Figure 3.17. Axial Force vs. Displacement for DT4 During the Full Test

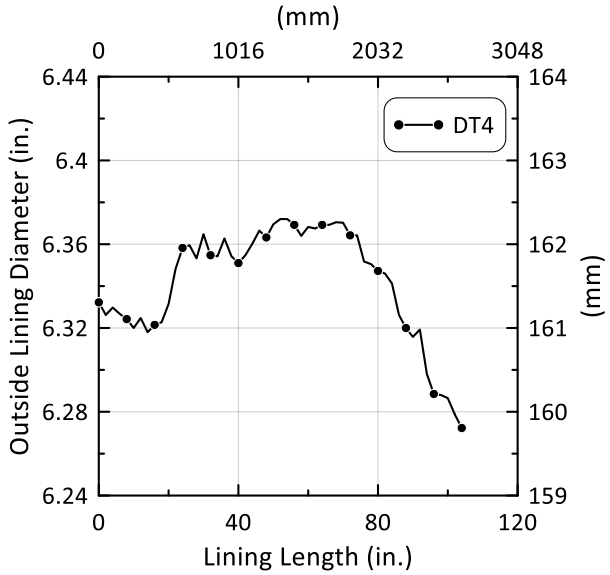

Figure 3.18. Average Outer Lining Diameter Along the North Section of the DT4 Specimen

Because the lining was cast and cured inside the pipe, the outside diameter of the lining is the inside diameter of the pipe. As the pipe was pulled along the lining, the smaller end of the pipe was pulled across a lining diameter that increased until a maximum at about 48 in. (1219 mm). Pulling a smaller diameter pipe along an increasingly larger diameter lining generated an axial load in the pipe that peaked at the location of the maximum lining diameter. After a pipe displacement along the pipe length of roughly 70 in. (1778 mm), corresponding to a crack opening of 70 in. (1778 mm), the lining diameter decreased rapidly, corresponding to rapidly decreasing axial force. When the end of the pipe was pulled along the lining past a lining diameter lower than that of the pipe, the axial force was rapidly approaching zero.

As the smaller diameter pipe was pulled across an increasingly larger diameter lining, the axial load increased. Increased axial load in the lining was accompanied by a load-induced reduction in lining diameter that caused the lining to lurch forward with decreasing axial load until the lining diameter increased again and came into contact

with the inside pipe diameter. Each axial load cycle was accompanied by a peak axial load and load-induced reduction in lining diameter as the lining lurched forward under constant pipe movement. As the lining lurched forward, it made firm contact with the pipe. Subsequent axial movement was accompanied by increased axial load until the next load cycle was initiated. During each cycle, there was an audible pop or boom as the lining lurched forward.

DT5

As indicated in Table 3.1, DT5 was performed with an 8.5-ft (2.6 m)-long specimen in the small load frame. It was initially tested with 80 psi (551 kPa) internal pressure at a sampling rate of 2 Hz. The testing protocol for DT5 was similar to that of DT4 and consisted of debonding followed by pipe displacement along the debonded lining at zero internal pressure.

Table 3.6 provides a list of the instrumentation used in DT5. The instrumentation for DT5 involved strain gages applied at 6 different locations both south and north of the crack at the center of the test pipe. Longitudinal strain gages at the crown and invert were established at two locations at 2 in. (51 mm) and 6 in. (152 mm) south and north of the gap. Circumferential strain gages at the crown were positioned at 2 in. (51 mm) and 36 in. (914 mm) south and north of the center of the pipe. Only longitudinal gages at the crown were placed at the other distances. Horizontal string pots were located at four different locations to measure the crack opening as well as any slip of the restraints. Pressure transducers were installed at the end cap and the deck to measure the internal pressure during the test.

Table 3.6. Instrumentation List for DT5

Location	Instrument Description	Local Instrument Name
36 in. South of Centerline	Crown, Axial Strain	-36C
	Crown, Circumferential Strain	-36CC
24 in. South of Centerline	Crown, Axial Strain	-24C
14 in. South of Centerline	Crown, Axial Strain	-14C
10 in. South of Centerline	Crown, Axial Strain	-10C
6 in. South of Centerline	Crown, Axial Strain	-6C
	Invert, Axial Strain	-6I
2 in. South of Centerline	Crown, Axial Strain	-2C
	Crown, Circumferential Strain	-2CC
	Invert, Axial Strain	-2I
2 in. North of Centerline	Crown, Axial Strain	2C
	Crown, Circumferential Strain	2CC
	Invert, Axial Strain	2I
6 in. North of Centerline	Crown, Axial Strain	6C
	Invert, Axial Strain	6I
10 in. North of Centerline	Crown, Axial Strain	10C
14 in. North of Centerline	Crown, Axial Strain	14C
24 in. North of Centerline	Crown, Axial Strain	24C
36 in. North of Centerline	Convert, Axial Strain	36C
	Crown, Circumferential Strain	36CC
Centerline	Horizontal String Pot	HSP_East
		HSP_West
Restraining Collars, North of Centerline		N_Slip
Restraining Collars, South of Centerline		S_Slip
End Cap	Pressure Transducer	Pressure_End_cap
Deck		Pressure_Deck
Actuator, South of Centerline	Actuator Displacement	Act-Disp

1 in. = 25.4 mm

Figure 3.19 (a) – (b) show photographs of the DT5 test specimen. Figure 3.19 (a) shows the pipe at the beginning of the test. Strain gages on the crown of the pipe and string pots along the eastern and western springlines of the pipe can be seen in the photo. Figure 3.19 (b) shows the leaking that occurred after approximately 0.3 in. (7.6 mm) of crack opening. The leaking was initiated when the debonding front propagated to the

south end of the pipe, breaking the end seal and causing water to flow longitudinally between the pipe and lining into the gap at the center of the specimen.

a) View of Specimen in Load Frame before Test Initiation

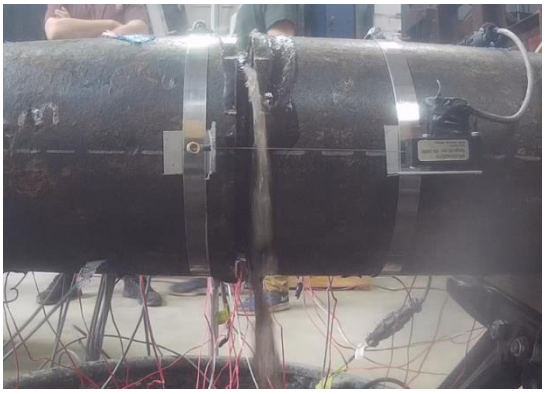

(b) View of Specimen Leaking after 0.3 in. (8 mm) of Crack Opening

Figure 3.19. Photos of the Test Specimen before and during the First Stage of DT5

Figure 3.20 shows both the internal pipe pressure and crack opening measured during the test plotted with respect to time. The test was paused from approximately 14 min to 20 min, during which time the pressure decreased to zero and the crack opening remained constant. At all other times the pipe pressure was maintained at approximately 80 psi (551 kPa). The gap opening was caused by displacement of the south pipe section relative to the lining. Thus, the gap opening is equivalent to the axial displacement of the south pipe. Figure 3.21 shows the axial force vs crack opening during debonding of the CI pipe from the Aqua-pipe lining. At 0.35 in. (9 mm) of crack opening and an axial force of 15.1 kips (67 kN), the pipe debonded to the south, causing a significant drop in axial force to 6 kips (26.6 kN).

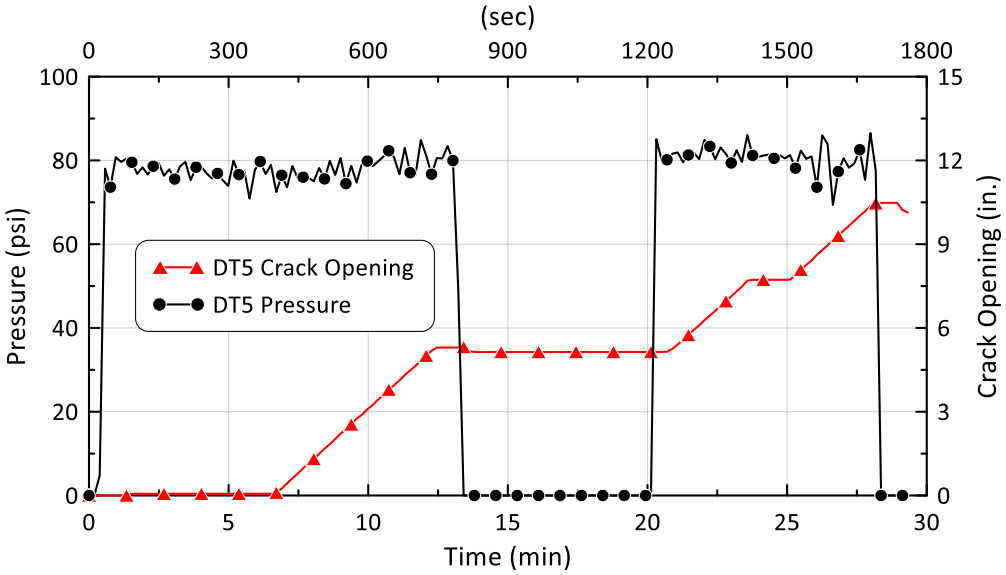

Figure 3.20. Pressure vs. Time During the First Stage of DT5

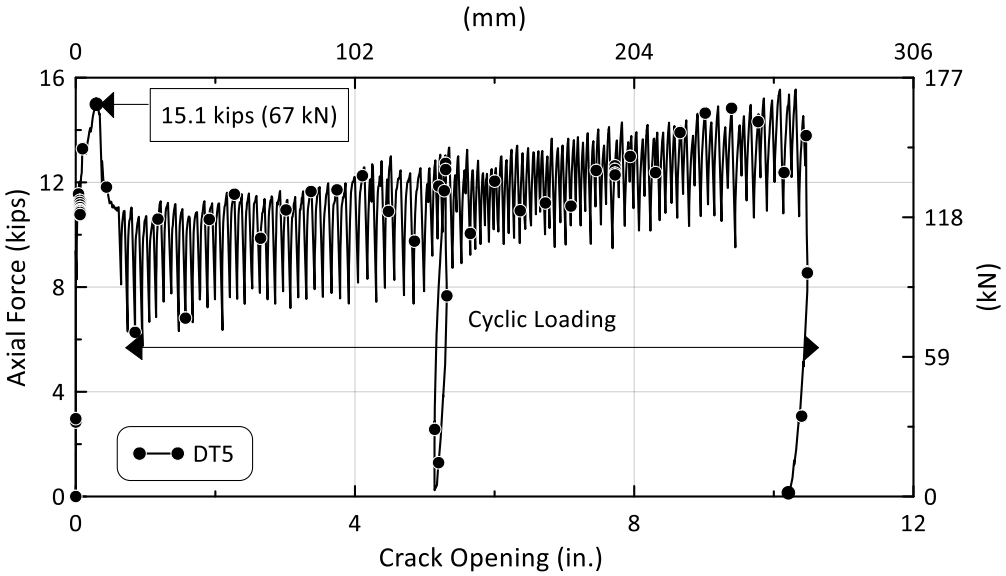

Figure 3.21. Axial Force vs. Crack Opening During the First Stage of DT5

The debonded length vs. crack opening was evaluated using strain gage data as explained for DT2. The relatively low sampling rate (2 Hz) for this test makes it more difficult to interpret the data so there is greater variability relative to the 50 Hz sampling rate used in DT2 (see Figure 3.11) when plotting debonded length vs. crack opening.

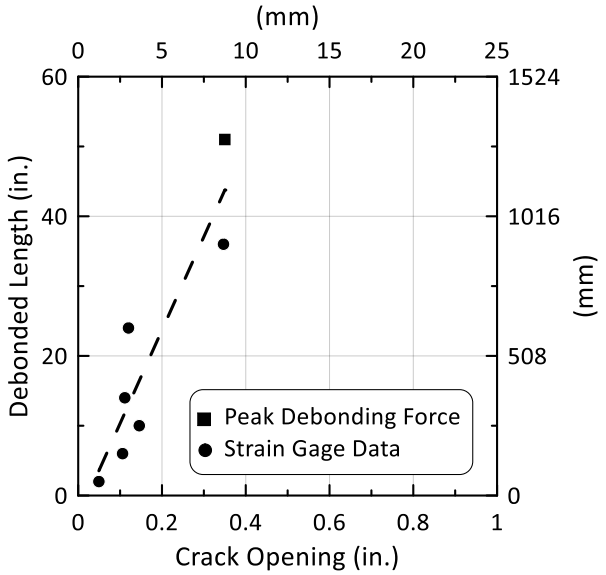

Figure 3.22. Debonding Front vs. Crack Opening for DT5 specimen

Figure 3.22 shows the debonded length estimated from the strain gage data plotted with respect to crack opening. The crack opening at the sudden drop in axial force in Figure 3.21 was correlated with the maximum debonding length of the pipe equal to 51 in. (1295 mm) and plotted in Figure 3.22. The data show that the debonding front moved rapidly through the pipe at a crack opening of approximately 0.35 in. (8 mm).

At approximately 11 in. (279 mm) of crack opening and an axial force of 15.1 kips (67 kN), the test was stopped due to significant leaking. The pipe specimen was moved to the large load frame, and oriented so that the debonded section was located north of the gap. The pipe was then pulled from the lining in a northward direction under no internal pressure.

Figure 3.23 shows the axial force vs. crack opening throughout the entire test. The crack opening was measured using actuator displacement. After the sudden drop in axial force at 0.35 in. (9 mm) of crack opening, the force increased steadily to 13 kips (58 kN) at about 5 in. (127 mm) of crack opening. The test was interrupted at 10 in. (254 mm) of crack opening and the specimen was moved to the large load frame.

After the test resumed in the large load frame, the axial force quickly increased to 10 kips (44 kN) and continued to increase to a maximum of 19.5 kips (87 kN) at 40 in. (1016 mm) of crack opening. This increase in axial force was accompanied by cyclic loading generated as the north section of the pipe was pulled along the lining. These cycles of axial force are shown in the force vs. crack opening plot. The greatest difference between maximum and minimum cyclic load occurred when a maximum force of 13.1 kips (58 kN) was measured at 40 in. (1016 mm) of gap opening.

Figure 3.24 shows the average outside lining diameter plotted with respect to distance along the lining. The diameter was measured from the center of the specimen at zero to near the end of the lining at 48 in. (1219 mm). As the pipe was pulled along the lining, the smaller end of the pipe was pulled across a lining diameter that increased until a maximum distance of 42 in. (1067 mm). Pulling a smaller diameter pipe along an increasingly larger diameter lining generated an axial load that peaked at the location of the maximum lining diameter. After a crack opening of 42 in. (1067 mm), the lining diameter decreased, corresponding to rapidly decreasing axial force.

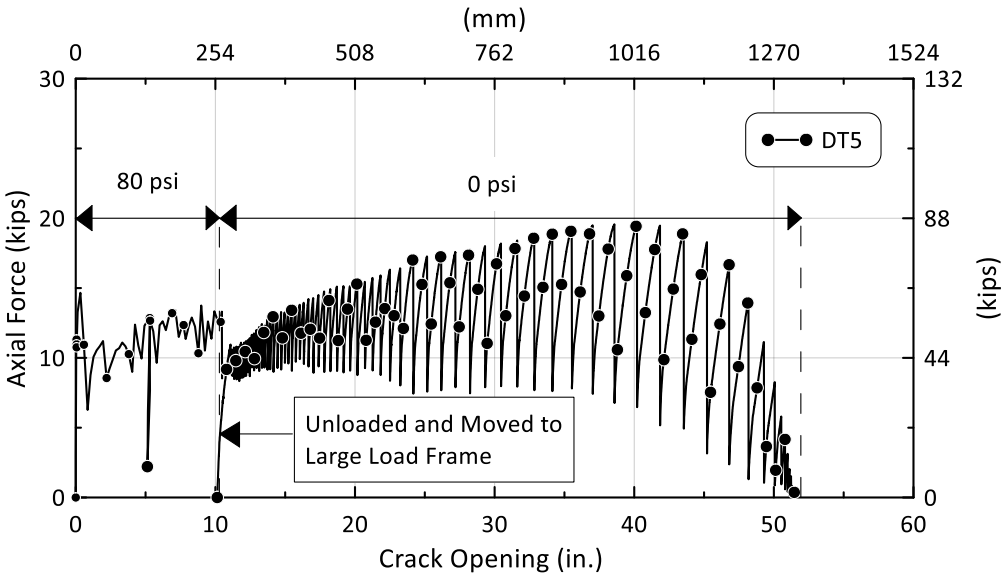

Figure 3.23. Axial Force vs. Crack Opening for DT5 Specimen

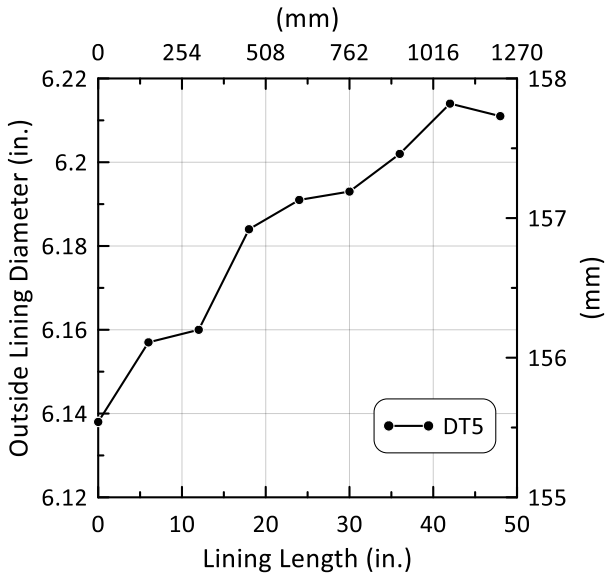

Figure 3.24. Average Outer Lining Diameter along the South Section of the DT5 Specimen

As discussed for DT2 and DT4, as the smaller diameter pipe was pulled across an increasingly larger diameter lining, the axial load increased. As explained for DT4, increased axial load was accompanied by a load-induced reduction in lining diameter that caused the lining to lurch forward, triggering a reduction in load and the beginning of another load cycle. Similar to DT4, there was an audible pop or boom during each load cycle during DT5.

DT6

As indicated in Table 3.1, DT6 was performed with an 8.5-ft (2.6 m)-long specimen in the small load frame. It was tested with 80 psi (551 kPa) internal pressure at a sampling rate of 25 Hz.

Table 3.7 provides a list of the instrumentation used in DT6. The instrumentation for DT6 involved strain gages applied at 6 different locations both south and north of the crack at the center of the test pipe. Longitudinal strain gages at the crown and invert

were established at two locations at 2 in. (51 mm) and 6 in. (152 mm) south and north of the gap. Circumferential strain gages at the crown were positioned at 2in. (51 mm) and 36 in. (914 mm) south and north of the center of the pipe. Only longitudinal gages at the crown were placed at the other distances. Horizontal string pots were located at four different locations to measure crack opening as well as any slip of the restraints. Pressure transducers at the end cap and the source on the deck to measure the internal pressure during the test.

Throughout DT6, there was substantial leaking from the beginning of the test. The leaking caused the internal pressure to drop from 80 psi (551 kPa) to approximately 20 psi (138 kPa) after 17 in. (432 mm) of crack opening. The test concluded after full debonding and 12 in. (305 mm) of pipe displacement to the south.

Figure 3.25 shows the internal pressure throughout the test superimposed on the crack opening. Virtually all gap opening was caused by displacement of the north pipe section relative to the lining. Thus, the gap opening is equivalent to axial displacement of the north pipe. The pressure was maintained at approximately 80 psi (550 kPa) until approximately 5 min into the test. At that time, pressure decreased due to extensive leaking. The leaking was caused by loss of seal at the end of the specimen, and continued until the test ended at approximately 17 in. (432 mm) of crack opening.

Figure 3.26 shows the axial force vs crack opening. The maximum axial force was 14.9 kips (66 kN). The strain gage data were used to estimate how the debonded length increased with crack opening in a manner similar to that applied for DT2, DT4, and DT5. The strain gage data and pressure show full debonding along the north section of pipe at 0.6 in. (15 mm) of crack opening. As the Aqua-pipe lining fully debonded from the DI pipe, the axial force decreased to approximately 3 kips (13 kN).

Table 3.7. Instrumentation List for DT6

Location	Instrument Description	Local Instrument Name
36 in. South of Centerline	Crown, Axial Strain	-36C
	Crown, Circumferential Strain	-36CC
24 in. South of Centerline	Crown, Axial Strain	-24C
14 in. South of Centerline	Crown, Axial Strain	-14C
10 in. South of Centerline	Crown, Axial Strain	-10C
6 in. South of Centerline	Crown, Axial Strain	-6C
	Invert, Axial Strain	-6I
2 in. South of Centerline	Crown, Axial Strain	-2C
	Crown, Circumferential Strain	-2CC
	Invert, Axial Strain	-2I
2 in. North of Centerline	Crown, Axial Strain	2C
	Crown, Circumferential Strain	2CC
	Invert, Axial Strain	2I
6 in. North of Centerline	Crown, Axial Strain	6C
	Invert, Axial Strain	6I
10 in. North of Centerline	Crown, Axial Strain	10C
14 in. North of Centerline	Crown, Axial Strain	14C
24 in. North of Centerline	Crown, Axial Strain	24C
36 in. North of Centerline	Convert, Axial Strain	36C
	Crown, Circumferential Strain	36CC
Centerline	Horizontal String Pot	HSP_East
		HSP_West
Restraining Collars, North of Centerline		N_Slip
Restraining Collars, South of Centerline		S_Slip
End Cap	Pressure Transducer	Pressure_End_cap
Deck		Pressure_Deck
Actuator, South of Centerline	Actuator Displacement	Act-Disp

1 in. = 25.4 mm

Figure 3.26 shows that, after debonding, the axial force continued to decrease with increasing crack opening. Following the procedures developed for DT2 and DT4 through DT6, the average outside diameter of the lining was measured and plotted along the length of the lining. The diameter was measured from the center of the test specimen at zero to near the end of the lining at 48 in. (1219 mm). As can be observed in Figure

3.27, the lining diameter decreases in the direction that the north pipe section was displaced across the test specimen. Thus, a larger pipe section diameter was pulled across a progressively smaller lining diameter, resulting in decreasing axial load similar to the response of DT2.

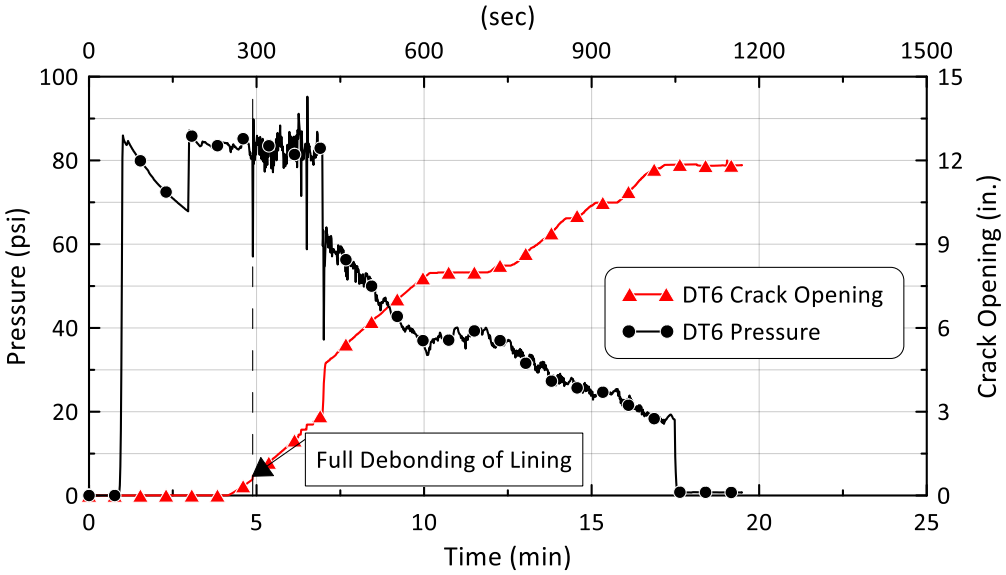

Figure 3.25. Internal Pressure vs. Time for DT6 Specimen

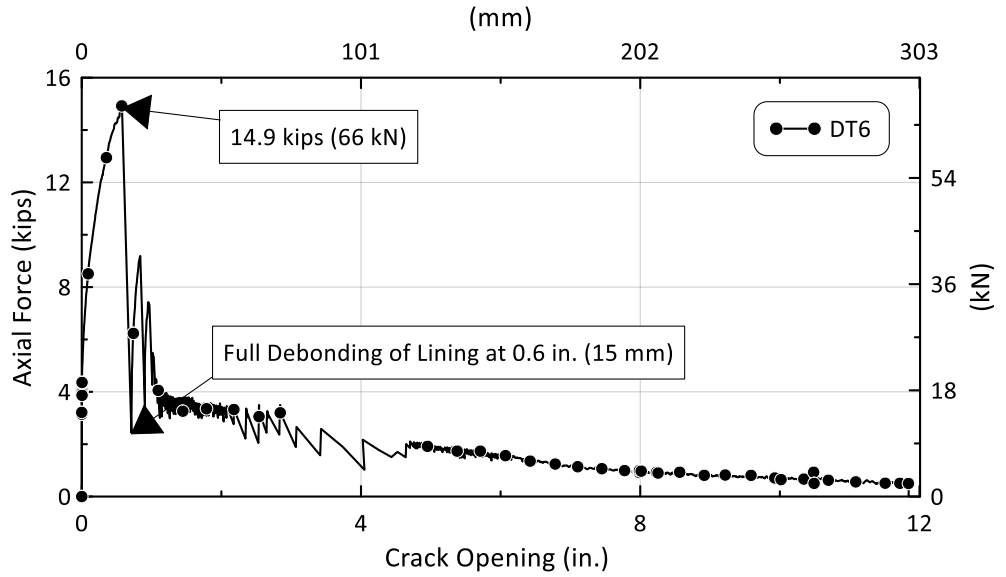

Figure 3.26. Axial Force vs. Crack Opening for DT6 Specimen

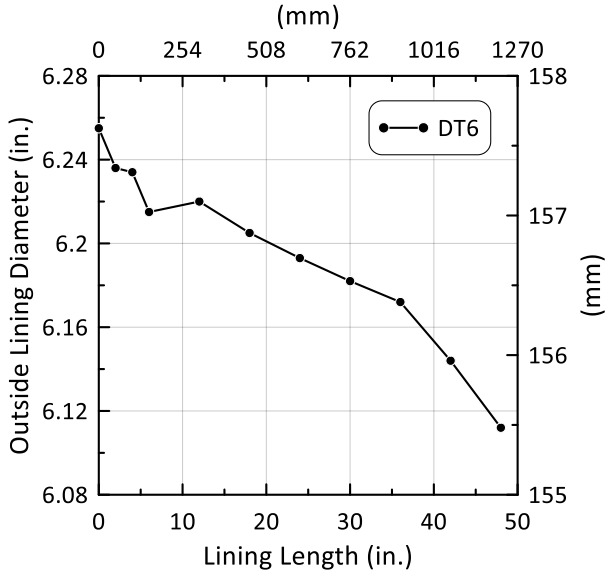

Figure 3.27. Average Outer Lining Diameter along the South Section of DT6

DT7

As indicated in Table 3.1, DT7 was performed with a 16-ft (4.57 m)-long specimen in the large load frame. It was tested with 80 psi (550 kPa) internal pressure at a sampling rate of 50 Hz. The test included debonding from the Aqua-pipe lining and pipe displacement along the debonded lining.

Table 3.8 provides a list of the instrumentation used in DT7. The instrumentation for DT7 involved strain gages applied at 9 different locations both south and north of the crack at the center of the test pipe. Longitudinal strain gages at the crown and invert were established at every location from 2 in. (51 mm) to 36 in. (914 mm) south and north of the gap. Circumferential strain gages at the crown and invert were positioned at 4 in. (102 mm) and 24 in. (610 mm) south and north of the center of the pipe.

Table 3.8. Instrumentation List for DT7

Location	Instrument Description	Local Instrument Name
72 in. South of Centerline	Crown, Axial Strain	-72C
60 in. South of Centerline	Crown, Axial Strain	-60C
48 in. South of Centerline	Crown, Axial Strain	-48C
36 in. South of Centerline	Crown, Axial Strain	-36C
	Invert, Axial Strain	-36I
24 in. South of Centerline	Crown, Axial Strain	-24C
	Crown, Circumferential Strain	-24CC
	Invert, Axial Strain	-24I
	Invert, Circumferential Strain	-24IC
12 in. South of Centerline	Crown, Axial Strain	-12C
	Invert, Axial Strain	-12I
8 in. South of Centerline	Crown, Axial Strain	-8C
	Invert, Axial Strain	-8I
4 in. South of Centerline	Crown, Axial Strain	-4C
	Crown, Circumferential Strain	-4CC
	Invert, Axial Strain	-4I
	Invert, Circumferential Strain	-4IC
2 in. South of Centerline	Crown, Axial Strain	-2C
	Invert, Axial Strain	-2I
2 in. North of Centerline	Crown, Axial Strain	2C
	Invert, Axial Strain	2I
4 in. North of Centerline	Crown, Axial Strain	4C
	Crown, Circumferential Strain	4CC
	Invert, Axial Strain	4I
	Invert, Circumferential Strain	4IC
8 in. North of Centerline	Crown, Axial Strain	8C
	Invert, Axial Strain	8I
12 in. North of Centerline	Crown, Axial Strain	12C
	Invert, Axial Strain	12I
24 in. North of Centerline	Crown, Axial Strain	24C
	Crown, Circumferential Strain	24CC
	Invert, Axial Strain	24I
	Invert, Circumferential Strain	24IC
36 in. North of Centerline	Crown, Axial Strain	36C
	Invert, Axial Strain	36I
48 in. North of Centerline	Crown, Axial Strain	48C
60 in. North of Centerline	Crown, Axial Strain	60C
72 in. North of Centerline	Crown, Axial Strain	72C
Centerline	Horizontal String Pot	HSP_East
	Horizontal String Pot	HSP_West

Table 3.8. Instrumentation List for DT7

Location	Instrument Description	Local Instrument Name
Restraining Collars, North of Centerline	Horizontal String Pot	North Slip
Restraining Collars, South of Centerline	Horizontal String Pot	South Slip
End Cap	Pressure Transducer	Pressure_Input
Water Hose		Pressure_Deck
Actuator, South of Centerline	Actuator Displacement	LSA1-Disp

1 in. = 25.4 mm

Only longitudinal gages at the crown were placed at a distance further than 36 in. (914 mm) from the crack. Horizontal string pots were located at four different locations to measure opening of the center gap as well as any slip of the restraints. Pressure transducers at the end cap and the source on the deck to measure the internal pressure during the test.

Figure 3.28 (a) – (b) show photographs of the DT7 test specimen. The test specimen has visible rust and pitting typical of a field specimen. Figure 3.28 (a) shows the pipe at the beginning of the test. Figure 3.28 (b) shows the specimen at the end of the test, including displacement in both the north and south directions from the initial crack location. During this test, the Aqua-pipe lining debonded completely to the north and then the north CI pipe was pulled over the Aqua-pipe lining to remove it from the lining.

Figure 3.29 shows a plot of internal pipe pressure vs. actuator displacement. Throughout the test, the pipe pressure was maintained with some fluctuation at 80 psi (551 kPa). This test differed from DT5 and DT6 where the pipe was pulled from the lining under diminished or near zero pressure. In DT7, axial movement of the pipe relative to the lining occurred under 80 psi (551 kPa) for the entire test.

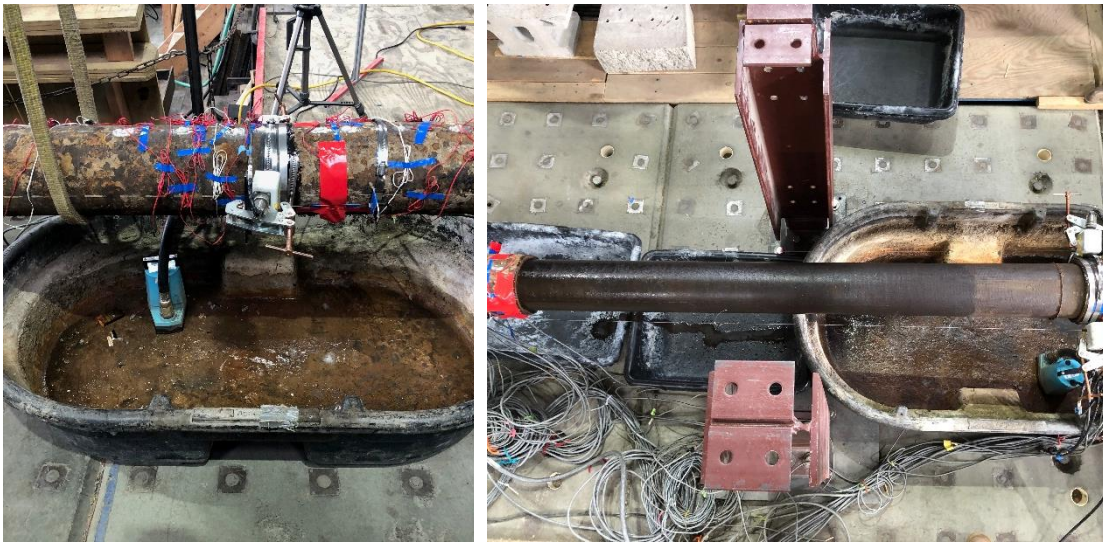

a) View of Specimen in Load Frame before Test Initiation

(b) View of Specimen at the end of the Direct Tension Test

Figure 3.28. DT7 Test Specimen before and after Direct Tension Test

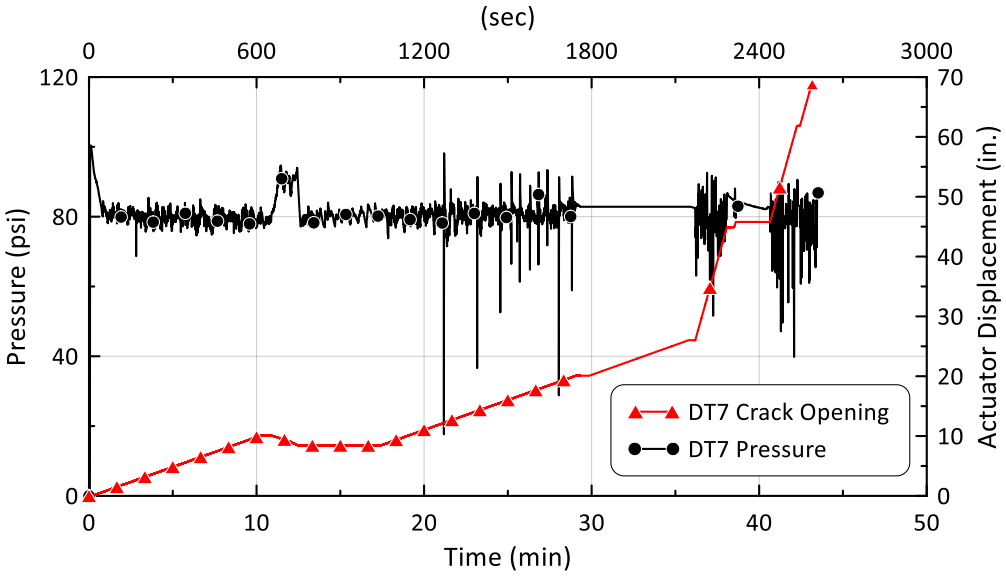

Figure 3.29. Pressure and Actuator Displacement vs. Time for DT7

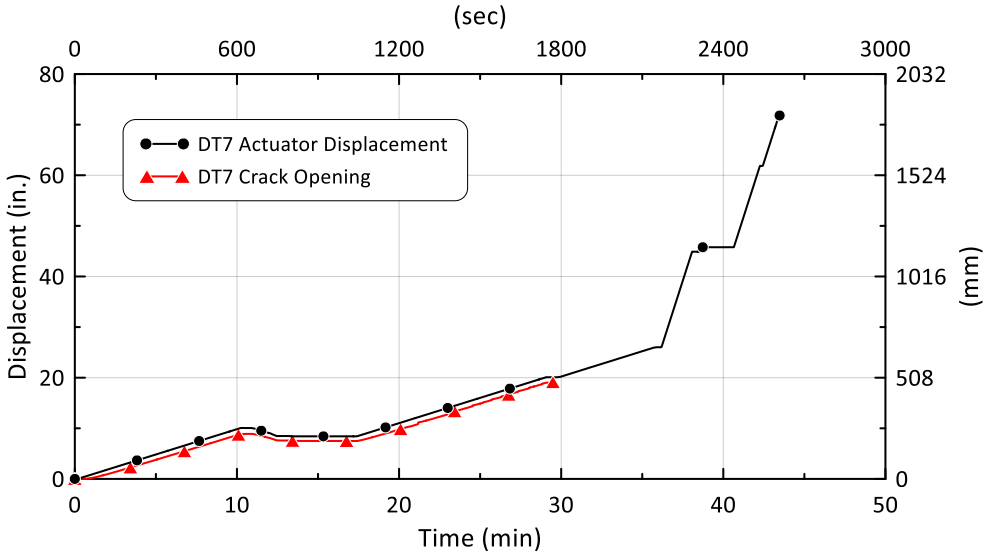

Figure 3.30. Actuator Displacement and Crack Opening vs. Time for DT7

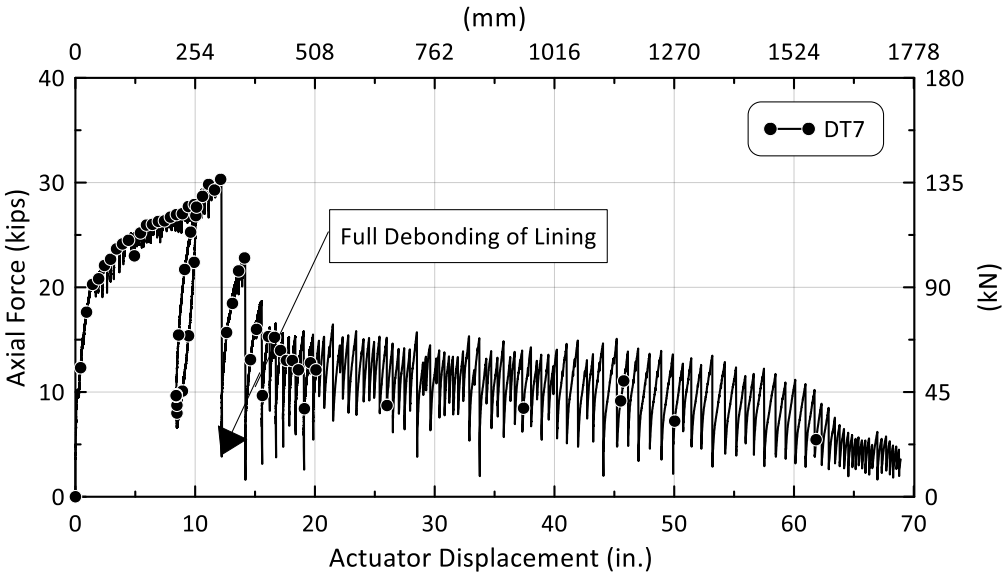

Figure 3.31. Axial Force vs. Actuator Displacement for DT7

Figure 3.30 shows the actuator displacement and crack opening vs. time. They recorded similar displacements until 30 min into the test, at which point the string pots reached their maximum travel. During the test, most of the crack opening developed as a result of the north section of the pipe debonding from the lining. Some debonding, however,

occurred in the south section of the pipe. At approximately 12 in. (305 mm) of actuator displacement, 2.7 in. (69 mm) of the displacement was axial movement of the lining from the south section of pipe.

Figure 3.31 shows the axial force vs. actuator displacement. The north pipe section debonded from the lining. At approximately 12 in. (305 mm) of actuator displacement, the force rapidly decreased to 6.5 kips (30 kN) during debonding, as it shows in the figure. At full debonding of the north pipe section, the pipe had been pulled 9.3 in. (236 mm) from the lining.

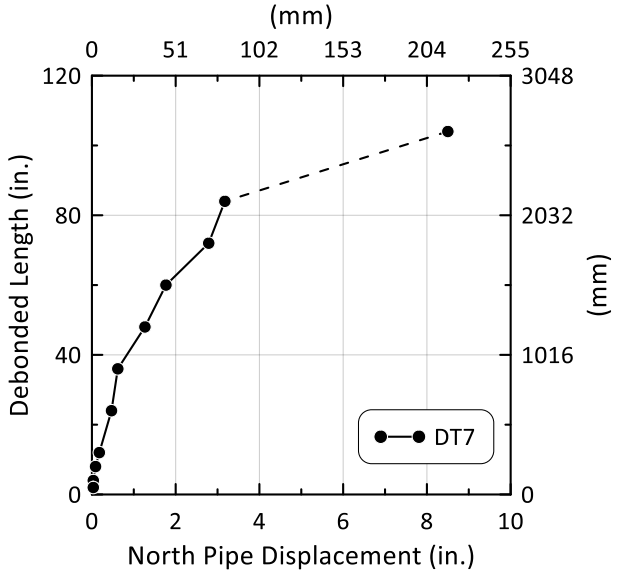

Figure 3.32. Debonding Length vs. North Pipe Displacement.

As shown in Figure 3.31, the axial force vs. actuator displacement plot can be divided into two broad episodes. The first episode involved the application of force to a maximum of 30 kips (133 kN) at which full debonding of the north pipe section occurred. The second episode involved displacement of the north pipe section relative to the lining from roughly 12 in. (305 mm) to about 70 in. (1778 mm), when the pipe was pulled from the lining. The axial force does not go to zero at the end of pipe

displacement because the force from the internal pressure was still recorded by the load cell.

Strain gage data were analyzed in a manner similar to that applied for DT2 and DT4 through DT6 to determine the location of the debonding front vs. axial displacement from the north pipe section. The actual displacement of the north pipe section was determined by subtracting the south pipe section displacement from the actuator displacement. As shown in Figure 3.32, the debonding front propagated rapidly through the north section of pipe to 84 in. (2134 mm) at a north pipe section displacement of 3.2 in. (81 mm). The increase in debonding length after 84 in. (2134 mm) is presented as a dashed line to indicate that there is uncertainty about the relationship between debonded length and north pipe section displacement from 84 to 104 in. (2134 to 2642 mm).

The actuator displacement was corrected to provide only the axial movement of the north pipe section after completion of debonding. Figure 3.33 is a plot of the axial force with respect to displacement of the north section of pipe after debonding occurred. After debonding there was no additional south pipe displacement and the maximum axial force remained around 14 kips (62 kN) until approximately 41 in. (1041 mm) of north pipe displacement. Then the maximum axial force decreased until a north pipe displacement of 66 in. (1676 mm).

Following the procedures developed for DT2, DT4, DT5, and DT6, the average outside diameter of the lining was measured and plotted along the length of the lining. The diameter was measured from the center of the test specimen at zero to near the end of the lining at 102 in. (2591 mm). At approximately 42 in. (1067 mm) from the center, the lining diameter peaks and begins to decrease. After a pipe displacement of 42 in. (1067 mm), a larger pipe diameter section moved over a lining with progressively

smaller diameters. This agrees with the decrease in axial force after 41 in. (1041 mm) of north pipe displacement seen in Figure 3.33.

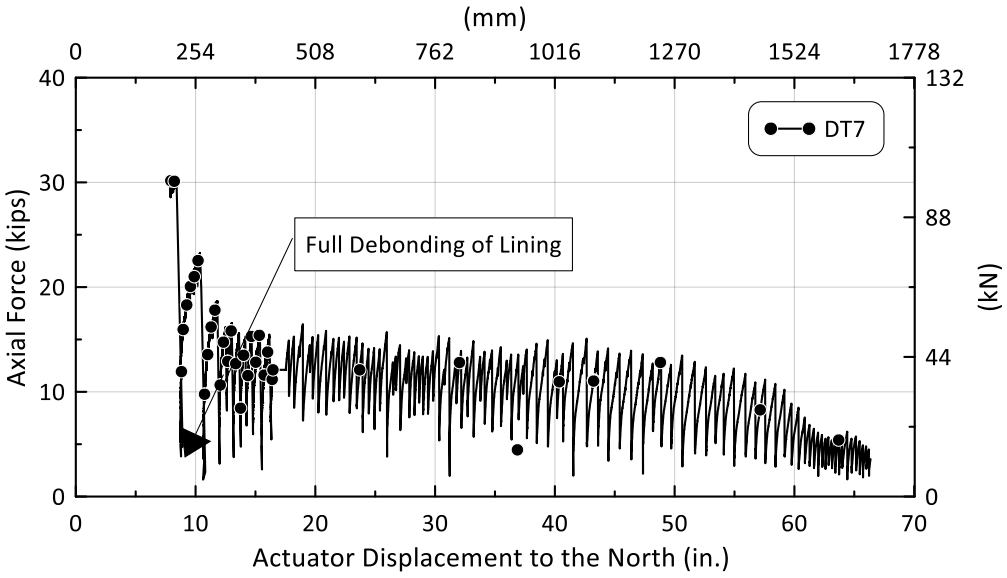

Figure 3.33. Axial Force vs. North Pipe Displacement after Debonding for DT7

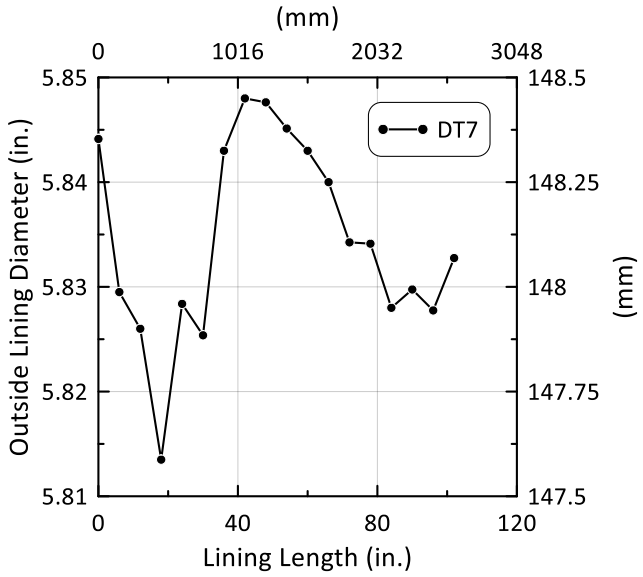

Figure 3.34. Average Diameter vs. North Pipe Section Length for the DT7 Specimen

Summary

The direct tension tests disclose a complex pattern of force vs. relative displacement between the Aqua-pipe lining and the host pipe. The mobilization of axial force is affected by fracture propagation, friction between the exterior surface of the lining and interior surface of the host pipe, and geometric resistance generated by relative movement of the lining within a pipe of variable inside diameter. The tests show that the initial load response to pipeline extension is dominated by a rapid rise in axial force as debonding between the lining and host pipe occurs. Previous research (Argyrou et al, 2018) has shown that the rapid rise in initial axial force can be modeled as a Type II fracture between the lining and inside pipe surface. The direct tension test results in this study show that the debonding force may be accompanied by relatively small additional frictional and geometric interference forces as the Type II fracture propagates.

The most important finding from the direct tension tests is that substantial additional axial forces may be mobilized after debonding as the lining is affected by geometric interference caused by movement through a pipe with variable internal diameter. The test results provide a first-time confirmation of this loading mechanism. Moreover, the test results show that geometric resistance caused by variable inside pipe diameter may be the dominant and controlling failure mechanism, depending on how the internal pipe diameter varies with distance along the pipeline.

After debonding, the axial force related to geometric conditions may result in decreasing or increasing loads. Because the lining is cast and cured inside the DI pipe, the outside diameter of the lining is the inside diameter of the pipe. As slip between the pipe and lining occur, the pipe may move along a lining of decreasing or increasing diameter. If the lining diameter decreases in the direction of relative movement, the axial load will decrease and geometric interference will not control failure. If the lining diameter

increases in the direction of relative movement, the axial load will increase and geometric interference may control failure.

DT2 and DT6 involve pipe movement in the direction of decreasing lining diameter, and the test results show low axial loads after debonding, followed by diminishing load with additional relative slip. In contrast, DT4, DT5, and DT7 involve pipe movement in the direction of increasing lining diameter, and the test results after debonding show increasing axial load with additional relative slip.

Figure 3.35 compares the axial force vs. displacement plots of DT4, DT5, and DT7. After debonding, all results show similar performance as the pipe was displaced along a lining of increasing diameter. Increasing axial loads were accompanied by tension-induced reductions in lining diameter that caused the pipe to lurch forward.

As the pipe moved, it came into firm contact with the lining. Subsequent axial movement was accompanied by increased axial load until the next load cycle was initiated. During each load cycle, there was an audible pop or boom that accompanied the abrupt forward displacement of the pipe.

The test results show a complex interaction involving the pipe and lining geometry, friction between the lining and pipe, and internal pressure. After debonding, DT4 and DT5 were performed at zero internal pressure. The highest maximum force after debonding was recorded in DT5. A larger change in pipe and lining diameter over distance was measured in DT5 than in DT4. DT7 was performed with the smallest change in pipe and lining diameter over distance. Although DT7 was performed under a pressure of 80 psi (551 kPa), it nonetheless shows the lowest axial load after debonding, which is apparently related to a smaller change of diameter compared with DT4 and DT5 specimens.

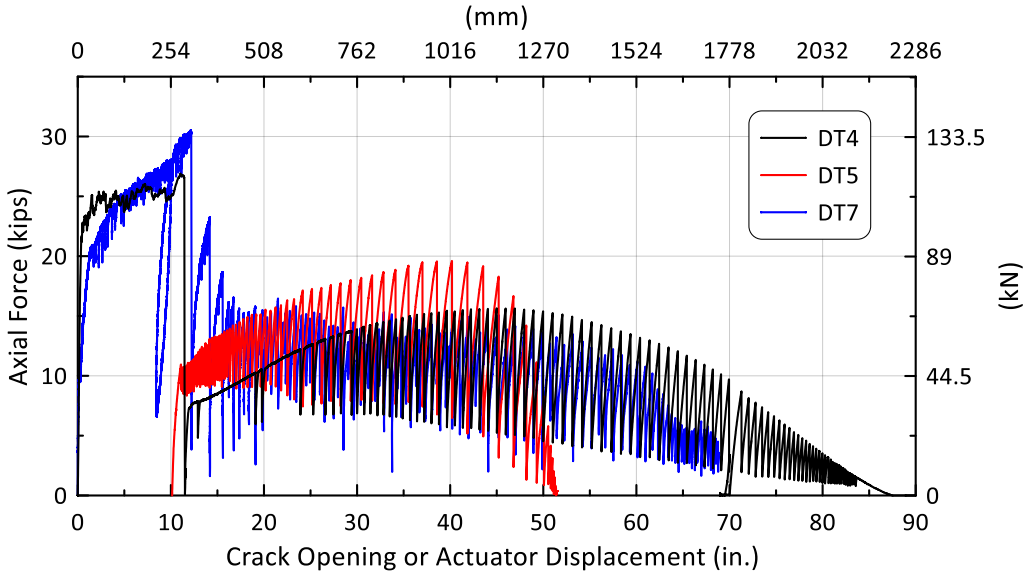

Figure 3.35. Axial Force vs. Crack Opening or Actuator Displacement for DT4, DT5, and DT7

To learn more about the relationship among axial force, internal lining pressure, and relative axial displacement, special friction tests were performed. These tests and their results are covered in the next section.

CHAPTER 4

FRICTION TESTS

Introduction

This section summarizes the results of special tests referred to as friction tests. These tests were designed to evaluate the influence of loading rate and internal lining pressure on the axial resistance to relative movement between the host pipe and Aqua-pipe lining. Friction tests were performed on the lining of the DT4 test specimen. The friction test specimen and test setup were configured from the DT4 specimen and modifications of the DT4 loading system.

Friction Test Setup

A plan view of the friction test setup is presented in Figure 4.1, and photographs of the setup are provided in Figure 4.2 and Figure 4.3. Two load frames consisting of steel plates attached to steel columns bolted to concrete bearing blocks were separated by 112.3 in. (2853 mm) center to center. The load frames supported and anchored the test pipes and Aqua-pipe lining. Figure 4.2 shows the test setup with the north and south load frames. Due to the high cyclic loads experienced during friction tests at relatively high internal lining pressure, the north and south load frames were stiffened and strengthened by inclined chains that were tensioned to resist axial loads developed on the 24-in. (610 mm)-long section of pipe as it was pulled in a northward direction along the lining.

The friction tests were performed after DT4 was completed. To set up for testing, the north section of pipe was pulled from the Aqua-pipe lining. The 102-in. (2591 mm)-long south section of the DT4 pipe and lining was fixed to the south load frame by means of restraining collars clamped to the pipes on either side of the load frame. This

arrangement is shown in the left side of Figure 4.1. The north load frame is located on the right (north) side of Figure 4.1. A 30-in. (762 mm)-long section of pipe and lining was fixed to the north load frame by restraining collars as shown in Figure 4.1. A 24-in. (610 mm)-long section of pipe was pulled from the south side of the exposed lining to the north load frame by means of steel rods connected to the restraining collars that were, in turn, attached to the mobile length of steel pipe. The steel rods were attached to the long stroke actuator on the north side of the north load frame. Although the full actuator and steel rods are not shown in Figure 4.1, they can be seen in Figure 4.2 and Figure 4.3.

Each friction test was performed from an initial position where the leading side of the 24-in. (610 mm)-long section of pipe was located 36 in. (914 mm) north of the DT4 specimen center. The pipe was then pulled along the lining 36 in. (914 mm) until contact with the north section of pipe. The moveable pipe section was then reset by pushing it under zero lining pressure back to its initial position. Figure 4.4 shows the movement of the 24-in. (610 mm)-long pipe section on the plot of the DT4 lining diameter vs. distance along the lining. As the pipe was pulled in the northward direction, it moved onto a lining that increased in diameter from 6.318 in. (160.5 mm) to 6.372 in. (161.9 mm) as shown in the figure.

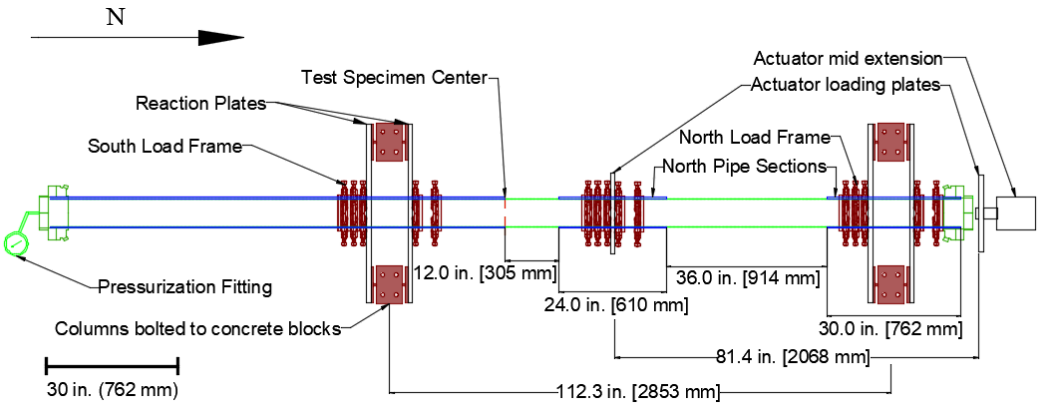

Figure 4.1. Plan View of Friction Test Setup

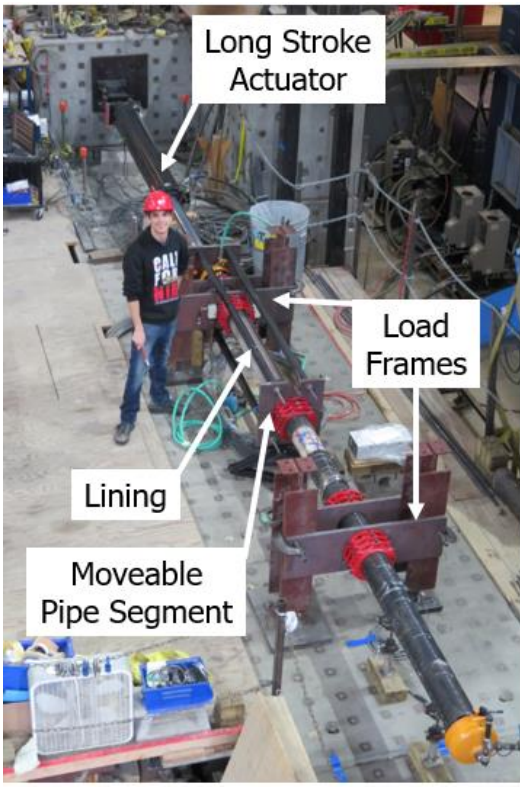

Figure 4.2. Photograph of Friction Test Setup (Facing North)

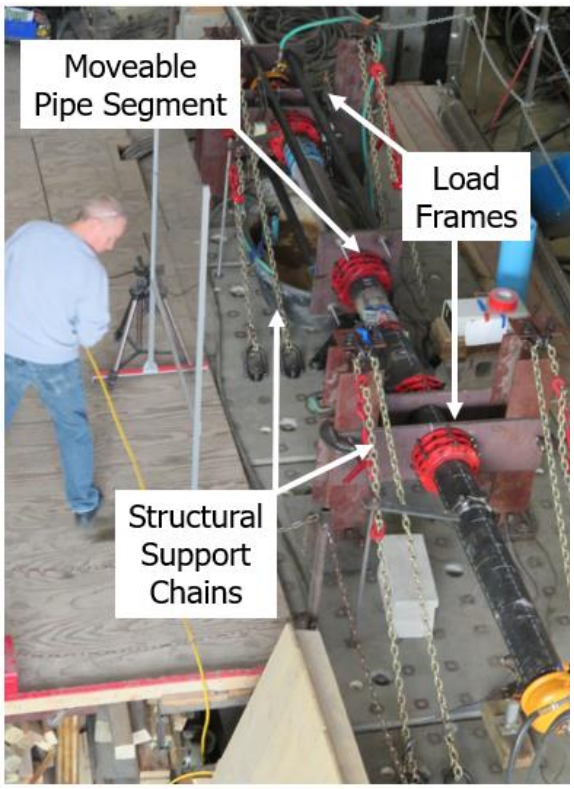

Figure 4.3. Photograph of Friction Test Setup with Structural Support Chains (Facing North)

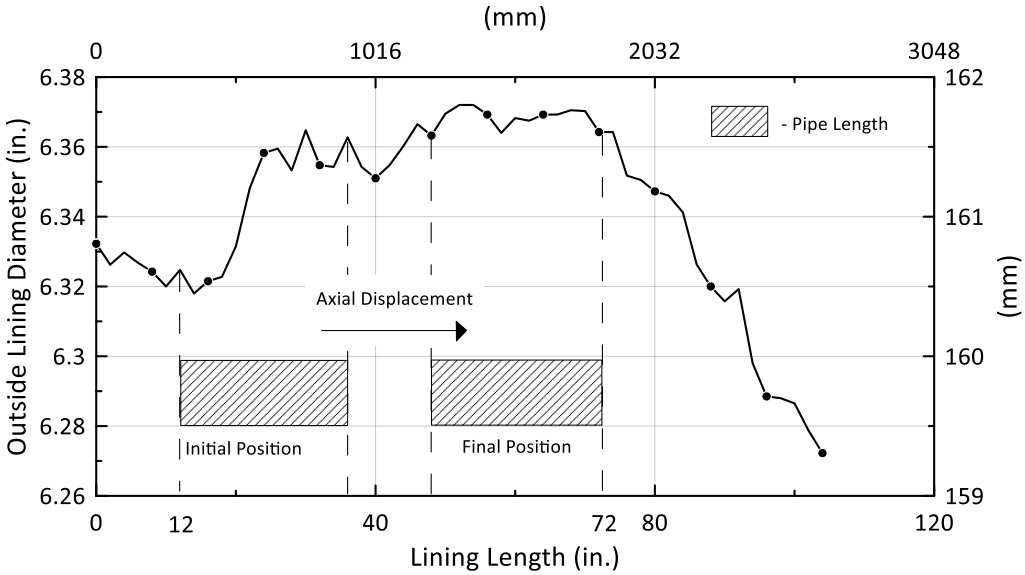

Figure 4.4. DT4 Specimen Outside Lining Diameter vs. Lining Length

The friction tests were performed under different loading rates corresponding to different rates of axial movement. They were also performed under different lining pressures. The pipe and lining system was sealed with end caps and pressurized through the fitting attached to the south end cap as shown in Figure 4.1.

Test Instrumentation

Axial and circumferential strain gages were located on the exterior surface of the pipe specimen at 6 in. (152 mm) from the gap at the center of the specimen. Horizontal string pots were used to measure displacement of the pipe as well as slip of the restraints. A list of the instrumentation used during the tests is presented in Table 4.1.

Table 4.1. Instrumentation List for Friction Tests

Location	Instrument Description	Local Instrument Name
6 in. North of Centerline	Crown, Axial Strain	6C
	Crown, Circumferential Strain	6CC
Actuator	Horizontal String Pot	HSP_Act_BU
Centerline		HSP_East
		HSP_West
Restraining Collars, North of Centerline		North Slip
Restraining Collars, South of Centerline		South Slip
End Cap	Pressure Transducer	Pres_Pipe
Deck		Press_Input
Centerline	Laser Extensometer	Laser_ext_5in
Actuator, South of Centerline	Actuator Displacement	LSA1-Disp

1 in. = 25.4 mm

Effects of Repeated Loading

Figure 4.5 presents the results of two friction tests performed under zero internal lining pressure. The axial force vs. pipe displacement are shown side by side for the first friction test (FT1) and a subsequent test (FT5) performed after intervening tests.

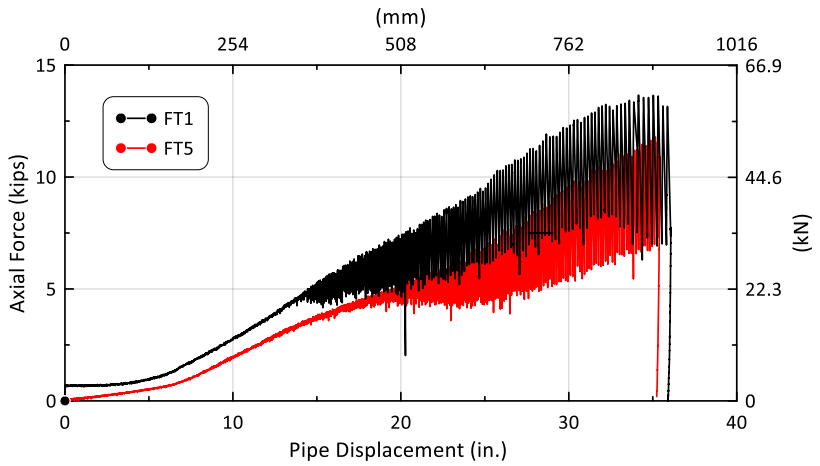

Figure 4.5. Axial Force vs. Pipe Displacement for the Initial Friction Test (FT1) and a Subsequent Friction Test (FT5)

The two tests were performed under identical conditions at a displacement rate of 1 in. (25 mm) per minute. Similar to the results of DT4 and DT5, during which a section of pipe was pulled along a lining of increasing diameter, the same cyclic loading phenomenon was observed with an audible pop or boom during each cycle. The loading cycles are shown in the figure.

The first test, FT1, shows a higher axial force at all displacements than the subsequent test, FT5. The FT1 maximum axial force is on average about 37% higher than the FT5 maximum force between displacements of 15 in. (381 mm) and 30 in. (762 mm). An axial force of 0.7 kips (3.1 kN) was required to initiate movement in FT1, whereas no initial force was required to induce axial displacement in FT5.

The reason for the higher force in FT1 is related to the roughness of the outside surface of the lining, which was more pronounced in the first test compared with subsequent tests. Repeated axial displacement during each friction test resulted in a smoother lining surface with lower frictional resistance compared to the initial test. Resistance to axial movement converged after the first test to steady state, repetitive values. Additional tests

run at the same pressure did not show significant differences in axial force vs. actuator displacement.

Load Rate Effects

Figure 4.6 compares the axial load vs. pipe displacement plots for three friction tests at zero lining pressure and three different rates of displacements of 1 in. (25 mm) per minute, 10 in. (250 mm) per minute, and 100 in. (2500 mm) per minute. The results of the three tests are nearly identical. For each test, both the maximum force and cyclic loading range follow closely the same load vs. displacement relationship.

These results show that axial load vs. displacement performances is not influenced by the loading rate. The load response remains unchanged over two orders of magnitude in displacement rate. Showing the independence of load response to the rate of loading displacement eliminates an important variable, and simplifies both the experimental conditions for relevant testing as well as the characterization of ground deformation effects on cured in place pipe behavior.

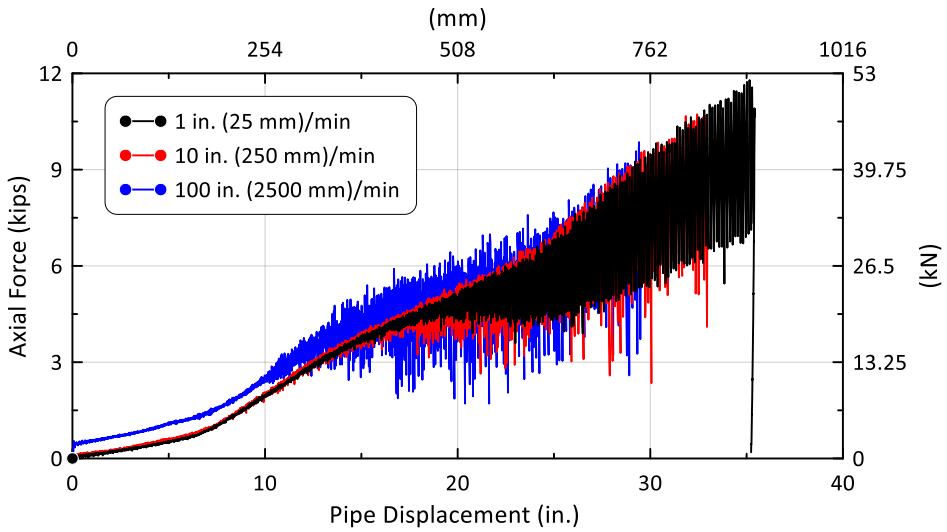

Figure 4.6. Comparison of Axial Force vs. Pipe Displacement Response at Zero Pressure for Different Loading Rates

Internal Pressure Effects

Figure 4.7 presents the load vs. pipe displacement plots at a constant loading rate of 10 in. (250 mm) per minute for nominal lining pressures of 0 psi, 25 psi (172 kPa), 50 psi (345 kPa), and 80 psi (551 kPa). There is a marked increase in axial force with increasing internal pressure at all levels of displacement.

To explore further the relationship between axial load and lining pressure, the pressures measured in each test are plotted with respect to pipe displacement in Figure 4.8 through Figure 4.10. Because of the cyclic loading and associated rapid changes in axial movement, it was difficult to maintain constant pressure. The trend in average pressures is plotted for each test, from which the pressure at any displacement can be identified and used to evaluate the relationship between peak axial load and internal lining pressure.

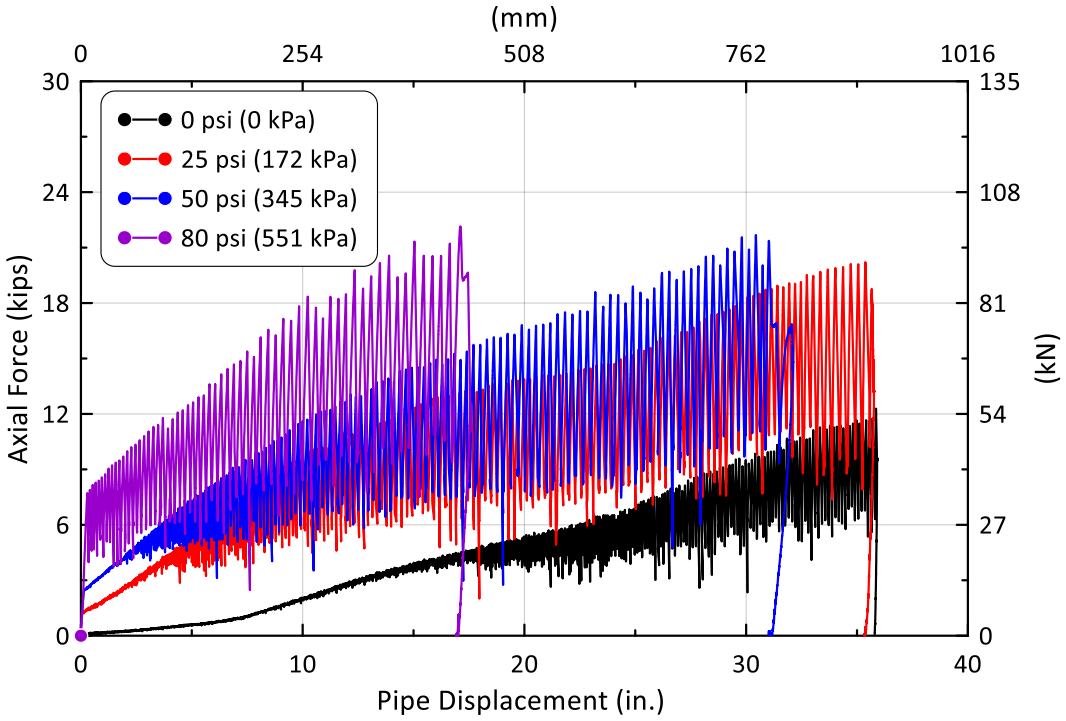

Figure 4.7. Load vs. Pipe Displacement Response at Different Lining Pressures and Constant Load Rate

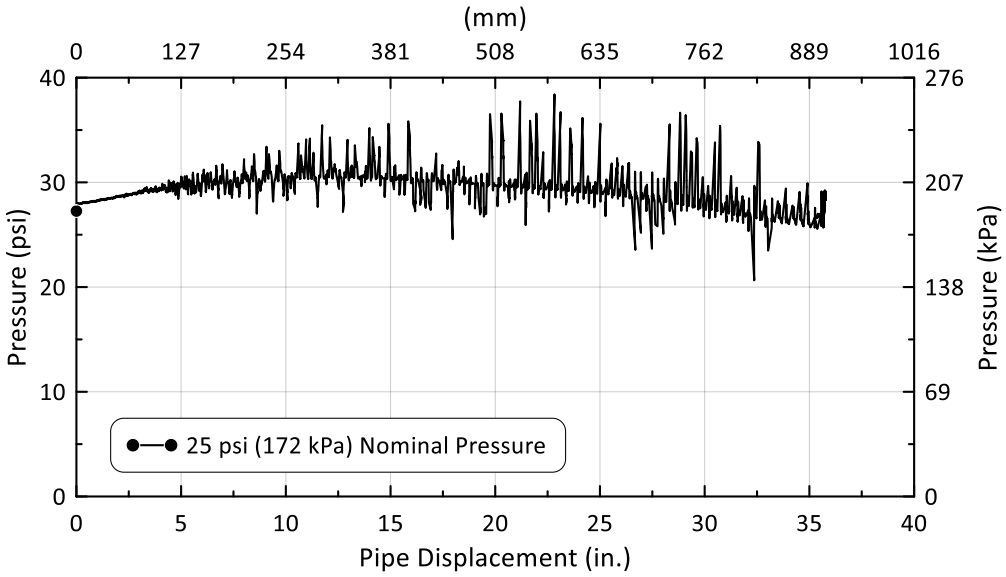

Figure 4.8. Lining Pressure vs. Pipe Displacement for Nominal 25 psi (172 kPa) Pressure

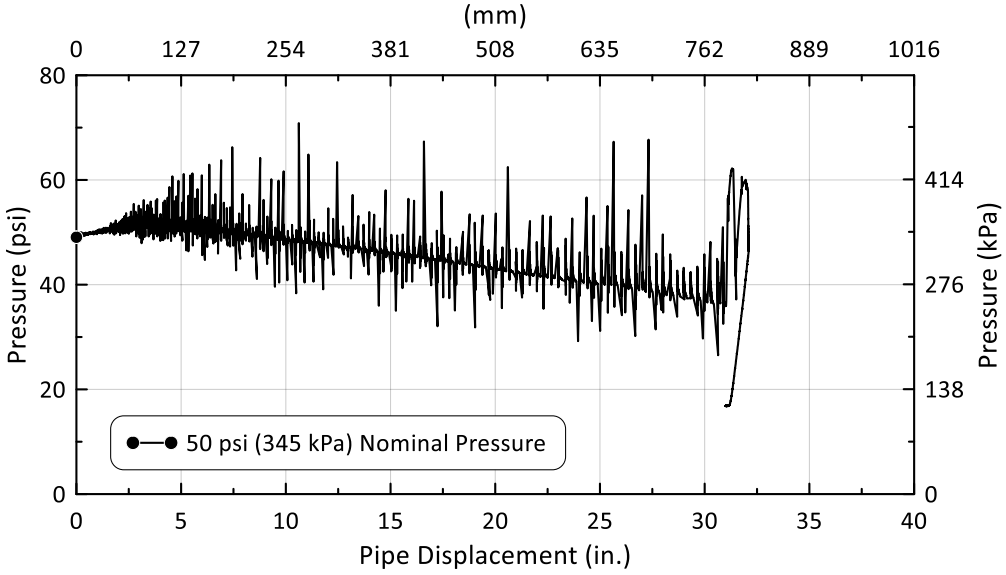

Figure 4.9. Lining Pressure vs. Pipe Displacement for Nominal 50 psi (345 kPa) Pressure

Figure 4.11 shows the peak axial load at 15 in. (381 mm) and 30 in. (762 mm) of pipe displacement plotted with respect to the internal lining pressure, both of which can be taken from Figure 4.7 through Figure 4.10. Given that the friction conditions and variation in lining diameter remain unchanged, the peak axial load at a given

displacement should increase in direct proportion to the internal lining pressure at the same displacement. This is indeed the case.

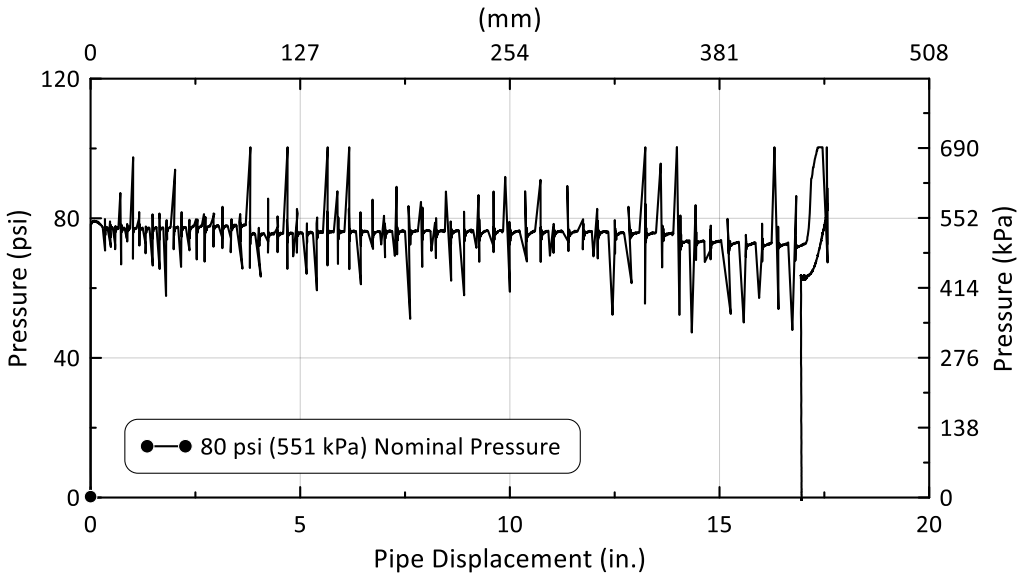

Figure 4.10. Lining Pressure vs. Pipe Displacement for Nominal 80 psi (551 kPa) Pressure

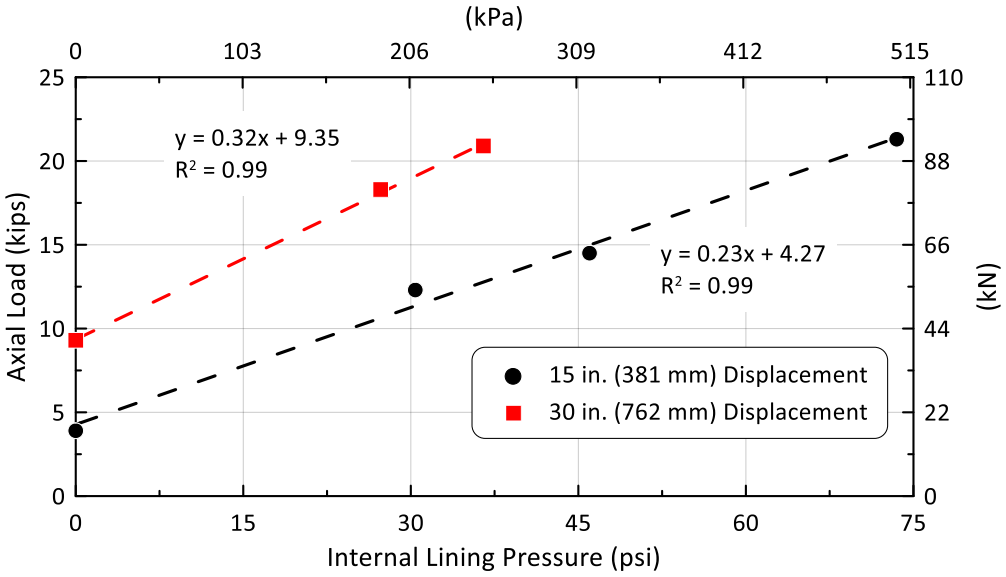

Figure 4.11. Axial Load vs. Internal Lining Pressure for Different Pipe Displacements

Figure 4.11 shows a linear relationship between axial load and lining pressure with similar slopes at two different levels of displacement. Although the data are sparse, the linear regression analyses show very high levels of R^2, which provides statistical support for the linear relationships.

Summary

The friction test results further define the force vs. relative displacement relationship between the Aqua-pipe lining and the DI host pipe first explored through the direct tension tests. Key findings include that the frictional resistance of the lining decreased after initial loading due to decreased surface roughness through repeated axial displacement between pipe and lining. When the specimen was loaded initially under zero pressure, the load response was higher due to greater surface roughness and frictional resistance. Subsequent tests exhibited a consistent, lower frictional resistance and axial load response than the first zero pressure test.

The friction tests show that the axial load response is independent of the loading rate. At varying loading rates, the axial loads experienced at each displacement were consistent in each test. The cyclic loading after debonding had a similar load range and maximum load for the tests conducted at 1 in. (25 mm)/min, 10 in. (250 mm)/min, and 100 in. (2500 mm)/min.

The most important result from the friction tests involves the influence of internal pressure on axial load response. As the internal pressure increased, the axial load for a given displacement increased linearly. Regressions of axial load vs. internal pressure at the same levels of displacement show a clear linear relationship with similar slopes.

CHAPTER 5

DIRECT SHEAR TESTS

Introduction

This section describes the direct shear test results for debonded Aqua-pipe lining and two variations in host pipe, involving new DI pipe and field CI pipe. The new DI pipe had a clean interior surface with an interface between the lining and host pipe that initially was rough and irregular. In contrast, the interface between the host pipe and Aqua-pipe lining in the CI field pipe samples was smooth, conspicuously lacking the initial roughness of the DI pipe. The CI field specimens were taken from pipe that Sanexen cleaned and installed with lining consistent with its field procedures.

The direct shear tests were performed to measure the shear forces required to slide the Aqua-pipe lining along a debonded length of pipe under various loads normal to the sliding surface. The ratio of shear to normal force is the coefficient of friction, f, of the interface between pipe and lining. The normal force for each test was calculated from the weight applied across the curved sliding surface using the correction process explained in Appendix A.

Direct Shear Test Setup and Procedure

The direct shear tests were performed on an MTS 858 Bionix Test System. Figure shows a schematic of the direct shear test setup including an actuator, pulley system, and test specimen. Figure shows a photo of the setup with a weight of 25 lb (0.11 kN) applied across the sliding surface. The hydraulic actuator had a stroke of 6 in. (152 mm) and a capacity of 5.5 kips (24.5 kN). The load cell had a capacity of 2.2 kips (9.8 kN).

Pipe specimens from DT1 and DT5 were used to create test specimens for the direct shear tests. A 45-degree section of the 6 in. (152 mm) diameter lined pipe was cut as

shown in Figure 5.3. a. The section was cut so that the lining was in contact with the interior pipe surface at the location where it was cured in place during installation. The lining was then separated from the host pipe as shown in Figure 5.3. b. The lining specimen was fixed to a wooden insert that was used to convey weights of various magnitude across the lining/pipe interface, as illustrated in Figure 5.2.

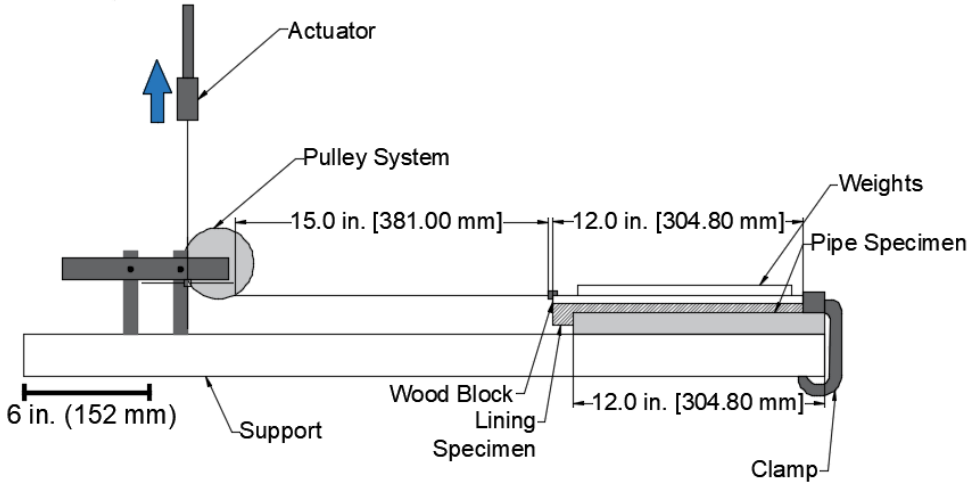

Figure 5.1. Schematic of Direct Shear Test Setup

Figure 5.2. Photo of Aqua-pipe Direct Shear Test Setup

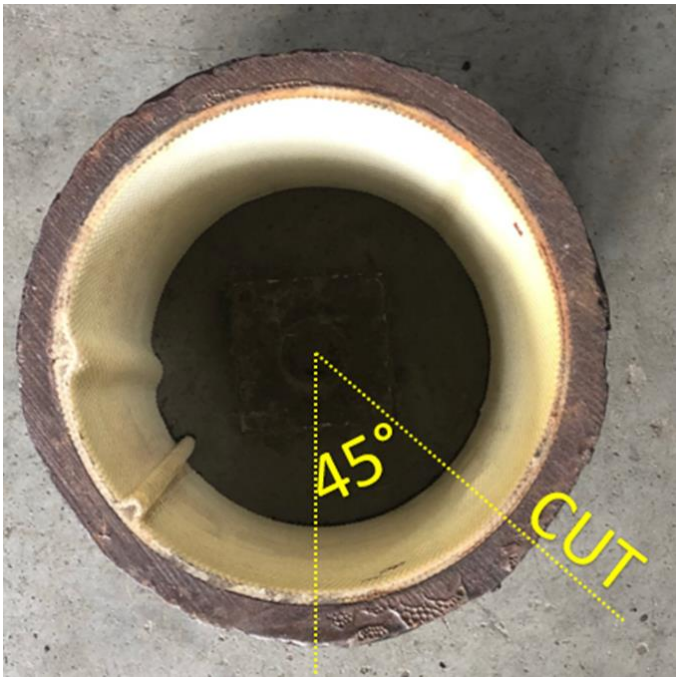

a) Specimen before it was Cut and the Lining and Host Pipe Separated

(b) View of Aqua-pipe Lining and Pipe Specimen after being Cut and Prepared

Figure 5.3. Photos of Aqua-pipe Direct Shear Test Specimen

To prepare for each test, the host pipe specimen was clamped to the table to prevent movement. The lining specimen fixed to the wooden block was attached to the pulley system and actuator. At the start of the test, the lining specimen was aligned with the clamp so that it was at its cured in place location with maximum contact surface between the lining and host pipe. The lining specimen was pulled across the host pipe for a distance of 3 in. (76 mm) to 6 in. (152 mm) at a displacement rate of 10 in. (254 mm) per minute, consistent with the displacement rate used in several friction tests. This procedure was repeated for four loading conditions for both the new DI and field CI specimens.

Experimental Results

Figure and Figure show the shear force vs. displacement for the new DI pipe and field CI pipe specimens, respectively, for weights of 50 lb (0.22 kN), 75 lb (0.33 kN), 100 lb (0.44 kN), and 200 lb (0.89 kN). The weights were converted to normal force following the procedure described in Appendix A. There was an overall downward trend in the shear force as the lining slid along the host pipe, reducing the contact between the lining and pipe surface.

For each test, the representative shear force for each normal force was calculated for a range of 0.5 in. (13 mm) to 3 in. (76 mm) of lining displacement relative to the host pipe. The shear force was plotted with respect to lining displacement. Using linear regression, the shear force at the midpoint of displacement at 1.75 in. (44.5 mm) was selected as the representative shear force for the applied normal force.

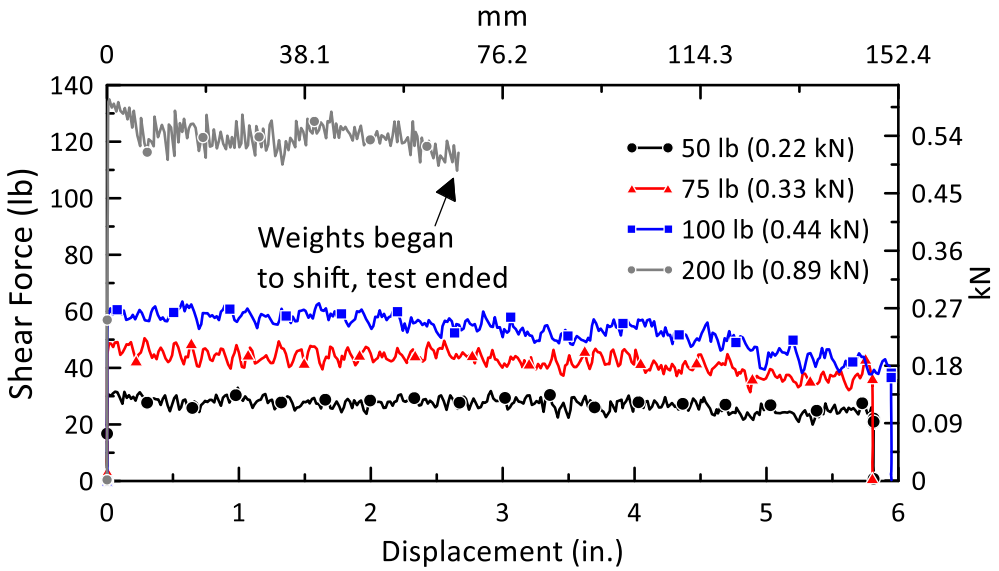

Figure 5.4. Shear Force vs. Displacement for Direct Shear Tests using New DI Pipe from DT1

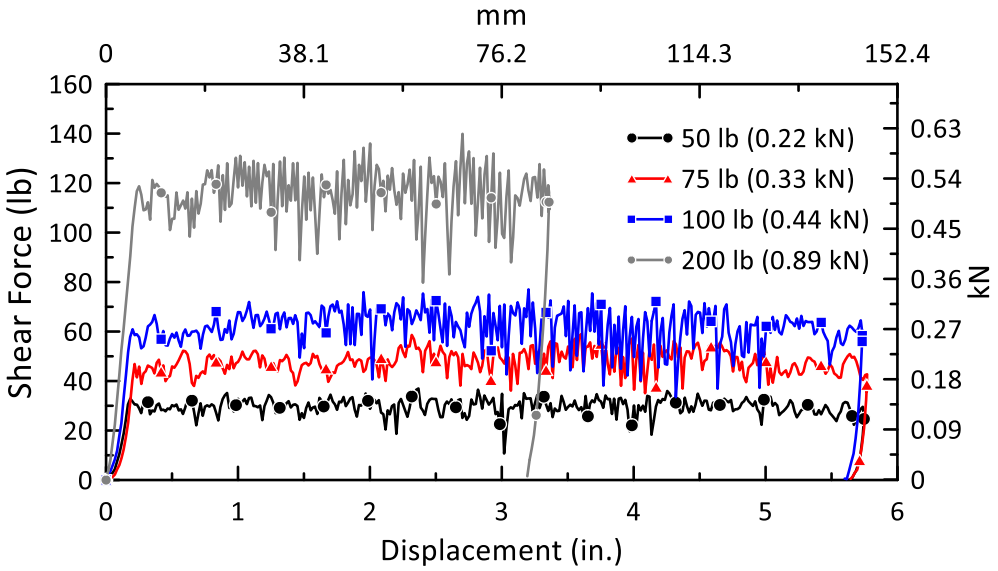

Figure 5.5. Shear Force vs. Displacement for Direct Shear Tests using Field CI Pipe from DT5

The shear force was plotted with respect to the normal force to determine the friction coefficient for each type of surface. 5.6 and Figure show linear regressions through zero of shear force vs. normal force for the new DI pipe and old CI pipe specimens, respectively. The friction coefficient is the ratio of shear force to normal force, so the slope of these plots represents the friction coefficient. The friction coefficient for the lining and both the new DI pipe and field CI pipe was 0.61.

Performing the direct shear tests involved repeated displacements of the lining along the host pipe, which promotes a smooth surface representative of field installation. The tests therefore provide the coefficient of friction that best matches field installation procedures.

To estimate the coefficient of friction representative of the initial roughness between the lining and new DI pipe, the results of FT1 and FT5 were used (see Figure 4.5). As described in Chapter 4, these tests were performed for Aqua-pipe lining in contact with new DI pipe.

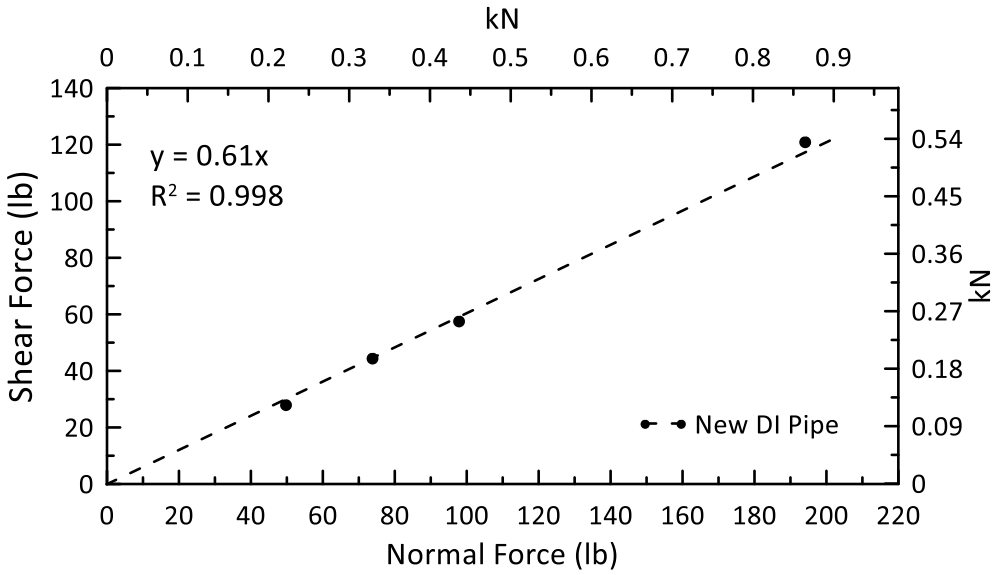

Figure 5.6. Shear Force vs. Normal Force for Direct Shear Tests Using New DI Pipe from DT1

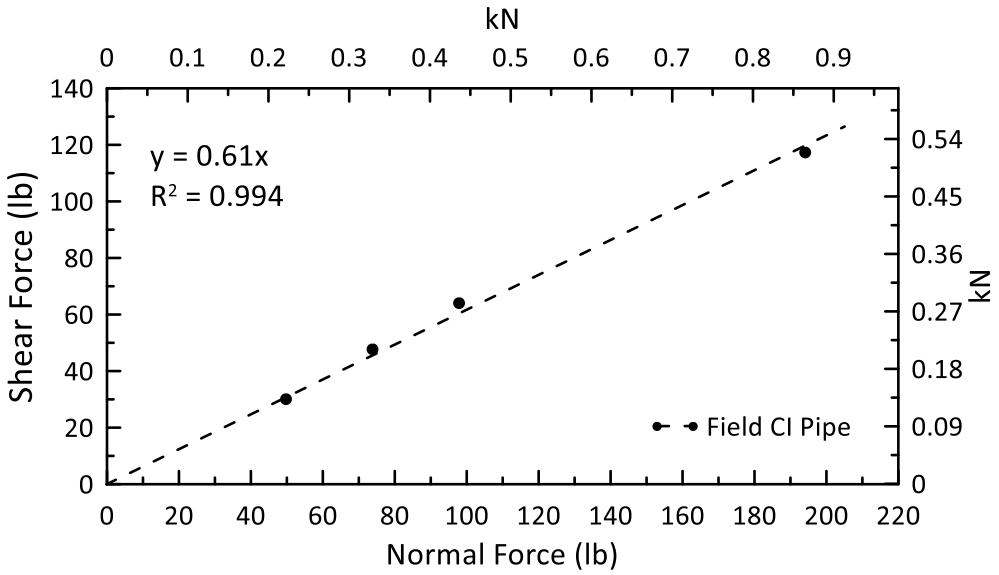

Figure 5.7. Shear Force vs. Normal Force for Direct Shear Tests Using Field CI Pipe from DT5

The reason for the higher axial force in FT1 is related to the increased roughness of the outside lining surface during the initial test. Both FT1 and FT5 were performed under

identical conditions of zero pressure, displacement rate, displacement, and pipe/lining geometry. Assuming that the main factor contributing to the different forces was friction, one can use the ratio of the peak axial loads in these two tests to estimate the coefficient of friction for the FT1 lining with initially high roughness. The weighted average ratio of axial force in FT1 with respect to FT5 at identical displacements is 1.37. Multiplying this ratio by f = 0.61 for smooth surface conditions provides an estimate of f = 0.84 for lining/pipe surfaces that are rough and irregular.

Summary

The results of the direct shear tests for new DI and field CI pipes show a coefficient of friction, f, of 0.61. This value represents the relatively smooth debonded lining surface conditions representative of the Sanexen cleaning and lining process for old CI water mains. It also represents the interface between the lining and new DI pipe after repeated displacements.

Using the ratio of peak axial loads in FT1 relative to FT5 one can estimate the coefficient of friction for the initially rough interface between the lining and DI pipe surface. Multiplying the weighted average ratio of 1.37 for the peak axial force in FT1 relative to FT5 at identical displacements with f=0.61 for a relatively smooth lining/pipe interface results in f = 0.84. This coefficient of friction provides an estimate for debonded lining/pipe interfaces that are rough and irregular.

CHAPTER 6

TEST SUMMARY

This thesis presents the results of tensile coupon tests on CIPP specimens, as well as full-scale tests of 6-in. (150 mm)-diameter pipe lined with CIPP. The CIPP used in this work is available commercially as Aqua-pipe, developed by Sanexen Environmental Services, Inc. The full-scale tests were designed to evaluate the performance of pipelines with CIPP under large axial deformation, including debonding between the lining and interior surface of CI and DI pipelines, axial force vs. displacement response in tension, and the relationship between axial force in the lining, internal pressure, and variation in pipe and lining diameter with respect to distance along the pipeline. The tests are part of a larger program to evaluate the performance of Aqua-pipe under earthquake-induced ground deformation.

The principal findings are summarized in this section with respect to tensile coupon tests, direct tension tests on full-scale specimens of DI and CI pipe lined with Aqua-pipe, and special friction tests designed to evaluate the relationship between axial lining force and internal lining pressure for conditions of axial slip between the lining and host pipe.

Tensile Coupon Test Results

Tensile coupon tests were performed on specimen of Aqua-pipe representative of longitudinal (warp) and circumferential (weft) directions of the lining. The test results show the average Young's modulus, Poisson's ration, and ultimate tensile strength and strain in the longitudinal direction of 390 ksi (2.69 GPa), 0.23, 10.9 ksi (75.2 MPa), and 15%, respectively. The test results show the average Young's modulus, Poisson's ration,

and ultimate tensile strength and strain in the circumferential direction of 414 ksi (2.86 GPa), 0.25, 15.3 ksi (106 MPa), and 11.1%, respectively.

The test results show that from zero to between 0.5% and 1.0% strain, the lining responds as a linear elastic solid. The Poisson's ratio is approximately 0.24 in both directions, and the difference in the Young's modulus is less than 7% lower in the warp than in the weft direction. In this range of tensile strain, the Young's modulus and Poisson's ratio are controlled principally by the epoxy. As the strain approaches and exceeds 1.0%, micro-fractures develop in the epoxy, and stress is transferred increasingly from the epoxy matrix to the fabric. This stress transfer results in a reduction of modulus. Moreover, the fabric stretches more in the warp direction than in the weft direction, where the strength of fibers is greater. As tensile strain exceeds approximately 5%, the fibers stretch and tighten, leading to increased modulus in both the warp and weft directions. The stiffness and strength in the weft direction exceed those in the warp direction due to the continuous nature of fibers in the weft direction.

Direct Tension Test Results

The direct tension tests disclose a complex pattern of force vs. relative displacement between the Aqua-pipe lining and the DI host pipe. The mobilization of axial force is affected by fracture propagation, friction between the exterior surface of the lining and interior surface of the host pipe, and geometric resistance generated by relative movement of the lining within a pipe of variable inside diameter. The tests show that the initial load response to pipeline extension is dominated by a rapid rise in axial force as debonding between the lining and host pipe occurs. Previous research (Argyrou et al, 2018) has shown that the rapid rise in initial axial force can be modeled as a Type II fracture between the lining and inside pipe surface. The direct tension test results in this

study show that the debonding force may be accompanied by relatively small additional frictional and geometric interference forces as the Type II fracture propagates.

The most important finding from the direct tension tests is that substantial additional axial forces may be mobilized after debonding as the lining is affected by geometric interference caused by movement through a pipe with variable internal diameter. The test results provide a first-time confirmation of this loading mechanism. Moreover, the test results show that geometric resistance caused by variable inside pipe diameter may be the dominant and controlling failure mechanism, depending on how the internal pipe diameter varies with distance along the pipeline.

After debonding, the axial force related to geometric conditions may result in decreasing or increasing loads. Because the lining is cast and cured inside the DI pipe, the outside diameter of the lining is the inside diameter of the pipe. As slip between the pipe and lining occur, the pipe may move along a lining of decreasing or increasing diameter. If the lining diameter decreases in the direction of relative movement, the axial load will decrease and geometric interference will not control failure. If the lining diameter increases in the direction of relative movement, the axial load will increase and geometric interference may control failure.

DT2 and DT6 involve pipe movement in the direction of decreasing lining diameter, and the test results show low axial loads after debonding, followed by diminishing load with additional relative slip. In contrast, DT4, DT5, and DT7 involve pipe movement in the direction of increasing lining diameter, and the test results after debonding show increasing axial load with additional relative slip.

The axial force vs. displacement plots of DT4, DT5, and DT7 show similar performance as the pipe was displaced along a lining of increasing diameter. Increasing axial loads were accompanied by tension-induced reductions in lining diameter that caused the

lining to lurch forward until firm contact with the pipe was reinstated. Subsequent axial movement was accompanied by increased axial load until the next load cycle was initiated. During each load cycle, there was an audible pop or boom that accompanied the abrupt relative displacement between the lining and the pipe.

The test results show a complex interaction involving the pipe and lining geometry, friction between the lining and pipe, and internal pressure. After debonding, DT4 and DT5 were performed at zero internal pressure. The highest maximum force after debonding was recorded in DT5. A larger change in pipe and lining diameter over distance was measured in DT5 than in DT4. DT7 was performed with the smallest change in pipe and lining diameter over distance. Although DT7 was performed under a pressure of 80 psi (551 kPa), it nonetheless shows the lowest axial load after debonding, which is apparently related to a smaller change of diameter compared with DT4 and DT5 specimens.

Friction Test Results

The friction test results further define the force vs. relative displacement relationship between the Aqua-pipe lining and the DI host pipe first explored through the direct tension tests. Key findings include that the frictional resistance of the lining decreased after initial loading due to decreased surface roughness through repeated axial displacement between pipe and lining. When the specimen was loaded initially under zero pressure, the load response was higher due to greater surface roughness and frictional resistance. Subsequent tests exhibited a consistent, lower frictional resistance and axial load response than the first zero pressure test.

The friction tests show that the axial load response is independent of the loading rate. At varying loading rates, the axial loads experienced at each displacement were consistent in each test. The cyclic loading after debonding had a similar load range and

maximum load for the tests conducted at 1 in. (25 mm)/min, 10 in. (250 mm)/min, and 100 in. (2500 mm)/min.

The most important result from the friction tests involves the influence of internal pressure on axial load response. As the internal pressure increased, the axial load for a given displacement increased linearly. Regressions of axial load vs. internal pressure at the same levels of displacement show a clear linear relationship with similar slopes.

Direct Shear Test Results

The results of the direct shear tests for new DI and field CI pipes show a coefficient of friction, f, of 0.61. This value represents the relatively smooth debonded lining surface conditions representative of the Sanexen cleaning and lining process for old CI water mains. It also represents the interface between the lining and new DI pipe after repeated displacements.

Using the ratio of peak axial loads in FT1 relative to FT5 one can estimate the coefficient of friction for the initially rough interface between the lining and DI pipe surface. Multiplying the weighted average ratio of 1.37 for the peak axial force in FT1 relative to FT5 at identical displacements with f = 0.61 for a relatively smooth lining/pipe interface results in f = 0.84. This coefficient of friction provides an estimate for debonded lining/pipe interfaces that are rough and irregular.

REFERENCES

Aqua-pipe (2018). “About Aqua-pipe”, Sanexen Water Inc. Emmaus, PA http://www.Aqua-pipe.com/about-us.html, Last accessed December 10, 2018.

ASTM International (2017). “Standard Test Method for Tensile Properties of Polymer Matrix Composite Materials”, *ASTM Standards.* D3039-17, pp. 1-13.

ASTM International (2014). “Standard Test Method for Tensile Properties of Plastics”, *ASTM Standards.* D638-14, pp. 1-17.

Argyrou C., Bouziou D, O’Rourke T.D. and Stewart H.E. (2018). “Retrofitting Pipelines with Cured-In -Place Linings for Earthquake-Induced Ground Deformations”, Soil Dynamics and Earthquake Engineering, 115: 156-168.

APPENDIX A

DETERMINATION OF NATURAL FORCE FOR DIRECT SHEAR TEST

Weight applied to a circular arc sliding surface must be resolved into its component normal to the sliding surface to evaluate friction. Figure A.1 is a transverse cross-section of a symmetrical semi-circular sliding surface, defined by radius, R, and the maximum angle, θ_{max}, relative to the vertical. θ_{max} is bounded from 0 to 90 degrees, which limits the geometry to a semi-circle.

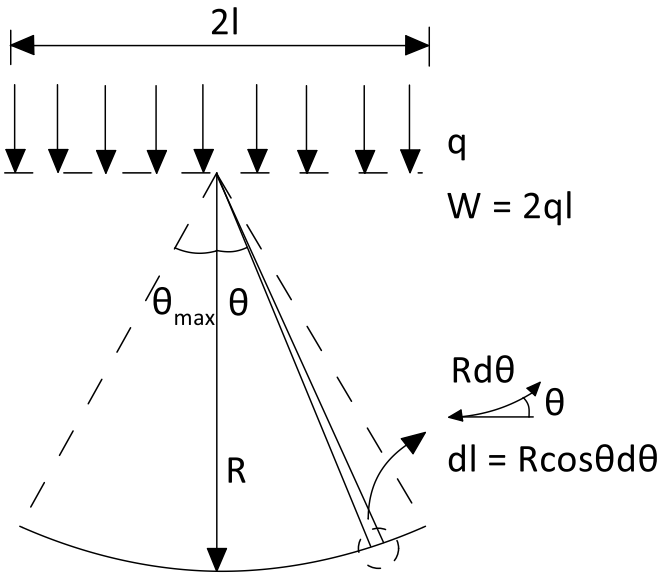

Figure A.1. Transverse Cross-section of a Uniformly Distributed Weight on a Circular Arc

The incremental weight, dW, applied to the sliding surface is

$$dW = qdl \tag{A.1}$$

in which q is the uniform vertical force per unit distance, and dl is the incremental half width over which the uniform vertical force is applied.

The incremental component of the weight normal to the sliding surface, dN, is

$$dN = dW\cos\theta = q\cos\theta dl \tag{A.2}$$

Referring to Figure A.1,

$$dl = R\cos\theta d\theta \tag{A.3}$$

Combining Eqns. A.2 and A.3 results in

$$dN = qR\cos^2\theta d\theta \tag{A.4}$$

The total force normal to the sliding surface is given by

$$N = 2\int_0^{\theta_{\max}} dN = 2qR\int_0^{\theta_{\max}} \cos^2\theta d\theta \tag{A.5}$$

that results in

$$N = 2qR\left(\frac{1}{2}\theta\right]_0^{\theta_{\max}} + \frac{1}{4}\sin(2\theta)]_0^{\theta_{\max}}\Bigg) \tag{A.6}$$

For the direct shear test specimens, $\theta_{max} = \pi/8$, from which

$$N = qD\left(\frac{\pi}{16} + \frac{1}{4}\sin(\pi/4)]\right) = 0.373qD \tag{A.7}$$

Recognizing that W= qDsin(π/8) and dividing Eqn. A.7 by W results in

$$N = \left(\frac{\pi/16 + 1/4\sin[\pi/4]}{\sin[\pi/8]}\right)W = 0.974W \tag{A.8}$$

When evaluating the coefficient of friction, f, from the direct shear test measurements, Eqn. A.8 allows one to calculate the force normal to the sliding surface. The normal for the direct shear test described in this report is converted from the weight as N = 0.974 W.